Molecular Medicine

Hematopoietic CC-Chemokine Receptor 2 (CCR2) Competent Cells Are Protective for the Cognitive Impairments and Amyloid Pathology in a Transgenic Mouse Model of Alzheimer's Disease

Gaëlle Naert and Serge Rivest

Laboratory of Endocrinology and Genomics, Centre Hospitalier de l'Université Laval (CHUL) Research Center and Department of Molecular Medicine, Faculty of Medicine, Laval University, Québec, Canada

Monocytes emigrate from bone marrow, can infiltrate into brain, differentiate into microglia and clear amyloid β (Aβ) from the brain of mouse models of Alzheimer's disease (AD). Here we show that these mechanisms specifically require CC-chemokine receptor 2 (CCR2) expression in bone marrow cells (BMCs). Disease progression was exacerbated in APP_{Swe}/PS1 mice (transgenic mice expressing a chimeric amyloid precursor protein (APPSwe) and human presenilin 1 (PS1)) harboring CCR2-deficient BMCs. Indeed, transplantation of CCR2-deficient BMCs enhanced the mnesic deficit and increased the amount of soluble Aβ and expression of transforming growth factor (TGF)-β1 and TGF-β receptors. By contrast, transplantation of wild-type bone marrow stem cells restored memory capacities and diminished soluble Aβ accumulation in APP_{Swe}/PS1 and APP_{Swe}/PS1/$CCR2^{-/-}$ mice. Finally, gene therapy using a lentivirus-expressing CCR2 transgene in BMCs prevented cognitive decline in this mouse model of AD. Injection of CCR2 lentiviruses restored CCR2 expression and functions in monocytes. The presence of these cells in the brain of non-irradiated APP_{Swe}/PS1/$CCR2^{-/-}$ mice supports the concept that they can be used as gene vehicles for AD. Decreased CCR2 expression in bone marrow–derived microglia may therefore play a major role in the etiology of this neurodegenerative disease.
Online address: http://www.molmed.org
doi: 10.2119/molmed.2011.00306

INTRODUCTION

Alzheimer's disease (AD) is a progressive and incurable disorder associated with a progressive decline of memory. This senile dementia is characterized by neuronal loss, synaptic degeneration, presence of extracellular amyloid-β-peptide (Aβ) deposits and intracellular neurofibrillary tangles. Amyloid precursor protein (APP) is cleaved into Aβ peptide, and two main Aβ isoforms exist ($Aβ_{1–40}$ and $Aβ_{1–42}$). Aβ peptide can oligomerize to form soluble oligomers (such as dimers, trimers or dodecamers [Aβ*56]) and aggregate to form protofibrils, fibrils and, then, amyloid plaques (1,2). Beside these pathological hallmarks, Aβ plaques are surrounded by microglia and astrocytes (3). Microglia, the mononuclear phagocytes of the brain (4), are found around Aβ plaques of brain sections taken from AD patients (5,6) and AD mouse models (7–9). Both resident microglia and newly differentiated cells that are derived from the bone marrow are frequently associated with Aβ deposits. Of interest, bone marrow–derived microglia restrict amyloid burden in the brain because of their more efficient phagocytic properties compared with their resident counterparts (7).

Microglia originate in part from hematopoietic cells and more particularly from monocytes (10–12). Monocytes express chemokine receptors and are distinguished by two subsets, namely a short-lived $CX_3CR1^{low}CCR2^{+}Gr1^{+}Ly6\text{-}C^{high}$ subset actively recruited to inflamed tissues and a $CX_3CR1^{high}CCR2^{-}Gr1^{-}Ly6\text{-}C^{low}$ subset (13). These chemokine receptors bind specific ligands and allow monocyte migration and attraction to their sites of production (14–16). CC-chemokine receptor 2 (CCR2) is found on the surface of monocytes and of a small percentage of T cells (17,18). Recently, it was shown that hematopoietic stem cells (HSCs) and hematopoietic progenitor cells express CCR2 (19) where it mediates the migration of mature monocytes from bone

Address correspondence to *Serge Rivest, Laboratory of Molecular Endocrinology, CHUL Research Center and Department of Anatomy and Physiology, Laval University, 2705, boulevard Laurier, Québec, Canada G1V 4G2. Phone: 418-654-2296; Fax: 418-654-2761; E-mail: serge.rivest@crchul.ulaval.ca.*
Submitted August 22, 2011; Accepted for publication November 28, 2011; Epub (www.molmed.org) ahead of print November 29, 2011.

The Feinstein Institute for Medical Research North Shore LIJ

marrow into the blood (20–22). This receptor also allows recruiting of circulating monocytes (22) and of HSCs and hematopoietic progenitor cells (19) to inflammatory tissues in mice. This occurs in mouse models of multiple sclerosis (23), in hippocampus at sites of axonal injury (24) and in systemic organs during inflammation (25). CCR2 can bind to five proinflammatory chemokines (monocyte chemoattractant protein [MCP]-1 to MCP-5), but its main physiological ligand is MCP-1 (also known as CCL2) (26). Several cell types express MCP-1, such as endothelial cells (27,28), astrocytes (29,30) and microglia (31–33). In addition to the property of binding only CCR2, MCP-1 is upregulated in the brain of both AD patients (34,35) and AD transgenic mice (7,36,37). Indeed, Aβ induces MCP-1 production in cultures of microglia (31,32) and astrocytes (29), and CCR2 deficiency accelerates the progression of AD hallmarks in two AD mouse models, namely APP Tg2576 mice (36) and APP_{Swe}/PS1 (37). CCR2 deficiency in APP_{Swe} (Tg2576) accelerates early disease progression and induces the premature death of the mice (36). In addition, APP_{Swe}/PS1/$CCR2^{-/-}$ mice exhibit earlier and aggravated mnesic impairment and an increase of soluble Aβ and plaque-associated microglia, which express, more importantly, transforming growth factor (TGF)-β1 and TGF-β receptors (37).

To address the contribution of $CX_3CR1^{low}CCR2^{+}Gr1^{+}Ly6\text{-}C^{high}$ monocytes in the etiology of AD, we used two complementary transplantations of CCR2-competent and -deficient bone marrow cells (BMCs) and overexpression of CCR2 transgene by BMCs in APP_{Swe}/PS1 and APP_{Swe}/PS1/$CCR2^{-/-}$ recipients. We show that CCR2-competent monocytes prevent disease onset as well as counteract AD pathology.

MATERIALS AND METHODS

Animals

Transgenic mice. We used adult male C57BL/6 mice (wild-type [WT]), green fluorescent protein (GFP) [CByJ.B6-Tg(CAG-EGFP)1Osb/J], $CCR2^{-/-}$ (B6.129S4-Ccr2tm1Ifc/J) and APP transgenic mice (APP_{Swe}/PS1) harboring the chimeric mouse/human β-amyloid precursor protein (APP695swe) and the human presenilin I (A246E variant) under the control of independent mouse prion protein promoter elements [B6C3-Tg(APP695)3Dbo Tg(PSEN1)5Dbo/J]. APP_{Swe}/PS1 mice were bred with the *CCR2*$^{-/-}$ mouse strain for at least three generations to generate APP_{Swe}/PS1/$CCR2^{-/-}$ triple transgenic animals. All mouse strains were purchased from The Jackson Laboratory (Bar Harbor, ME, USA) and maintained in a C57BL/6J background. All newborn pups were genotyped as described in The Jackson Laboratory protocol. Mice were used to study behavioral and biochemical modifications at 6 months of age. Mice were housed three to five per cage and acclimated to standard laboratory conditions (12-h light, 12-h dark cycle; lights on at 07:00 and off at 19:00) with free access to mouse chow and water. Animal breeding and experiments were conducted according to the Canadian Council on Animal Care guidelines, as administered by the Laval University Animal Care Committee.

Chimeric mice: irradiation and bone marrow transplantation. Male APP_{Swe}/PS1 and APP_{Swe}/PS1/$CCR2^{-/-}$ mice, 2.5–3 months of age, were exposed to 10 Gy total-body irradiation using a ^{60}Co source (Theratron-780 model, MDS Nordion, Ottawa, ON, Canada). A few hours later, the animals were injected via a tail vein with approximately 5×10^6 BMCs freshly collected from male GFP or $CCR2^{-/-}$ mice. APP_{Swe}/PS1 and APP_{Swe}/PS1/$CCR2^{-/-}$ mice received WT GFP cells and another group of APP_{Swe}/PS1 received $CCR2^{-/-}$ cells (n = 10–13 by group). As previously described (38), cells were aseptically harvested by flushing femurs with Dulbecco's phosphate-buffered saline (DPBS) containing 2% fetal bovine serum (FBS). Cell samples were combined for each genotype, filtered through a 40-μm nylon mesh, centrifuged and passed through a 25-gauge needle. Recovered cells were resuspended in DPBS at a concentration of 5×10^6 viable nucleated cells per 200 μL. Irradiated mice transplanted with the cell suspension were housed in autoclaved cages and treated with antibiotics (0.2 mg trimethoprim and 1 mg sulfamethoxazole/mL drinking water given for 7 d before and 2 wks after irradiation). Animals (n = 77) were submitted to behavioral tests 3 months after transplantation and then killed for brain analyses.

Production and femoral injection of lentiviral vectors. Lentivirus construction was performed as previously described (39), using a ViraPower T-Rex Lentiviral Gateway Vector kit (Invitrogen, Burlington, ON, Canada). The vector pLenti4/TO/V5-DEST was modified to visualize transduction. The Zeocin resistance cassette was replaced by the enhanced GFP coding region with a phosphoglycerate kinase promoter. The insert was amplified using the pSuperior vector as a template (OligoEngine) (forward, 5′-CACAAGTGGCCTCGAGCCTC GCACACATTCCACATCCAC-3′; reverse, 5′-CTTGTTCAATCATGGTACCT CTAGCCTTAAGTTCGAGAC-3′) and was inserted in the pLenti4/TO/V5-DEST between the *Xho*I and *Kpn*I restriction sites, forming the pLenti/GFP vector. The *CCR2* coding sequence was amplified by polymerase chain reaction (PCR) from a cDNA brain library and cloned in the pENTR4 vector using the *Xmn*I and *Xho*I restriction sites of the polylinker (forward, 5′-ATGGAAGACA ATAATATGTTACCTC-3′; reverse, 5′-CAAACTGTCACTCGAGTTACAACC-3′; GenBank accession number NM_009915). The *CCR2* coding sequence was transferred onto the pLenti/GFP downstream of the cytomegalovirus promoter by homologous recombination, forming the pLenti/GFP/CCR2. To prepare the lentivirus, 293T cells (a gift from L Vallières, Laval University, Québec, Canada) were transfected with pLenti/GFP/CCR2, pLPI, pLP2 and pLP–vesicular stomatitis virus protein G (20 μg per plasmid) using the calcium chloride technique. Lentiviruses were concentrated by ultracentrifugation (50,000*g* for 2 h) of the 72-h culture supernatant and resuspended in

Dulbecco's modified Eagle's medium (Sigma, Oakville, ON, Canada). Male APP_{Swe}/PS1 and APP_{Swe}/PS1/$CCR2^{-/-}$ mice (2.5–3 months of age) were anesthetized with isoflurane, and the knees were flexed successively. Each intrafemoral space was reached with a 28-gauge needle by applying gentle twisting and pressure between the condyles at the top of the femur. Then 20 μL of the lentiviral suspension (2×10^7 lentiviruses) was injected in each femur with a 30-gauge needle. APP_{Swe}/PS1 and APP_{Swe}/PS1/$CCR2^{-/-}$ mice treated with control lentivirus (pLenti/GFP) or pLenti/GFP/CCR2 were tested at 6 months of age for spatial learning and memory and then killed for brain analyses (n = 59).

Behavioral Analyses

Water T-maze. Mice were tested during the "light-on" phase of the day. Mice of each group were tested in a same session. The behavioral experimenter was blind to the genetic and treatment status of animals. To assess hippocampal-dependent spatial learning and memory, mice were trained in the water T-maze task. In this paradigm, we evaluate the mouse's ability to remember the spatial location of a submerged platform. The T-maze apparatus (stem length, 64 cm; arm length, 30 cm; width, 12 cm; wall height, 16 cm) was made of clear fiberglass and filled with water (23 ± 1°C) at a height of 12 cm. A platform (11 × 11 cm) was placed at the end of the target arm and was submerged 1 cm below the surface. The acquisition phase allows evaluation of the animals for left–right spatial learning. During the first two trials, platforms were placed on each arm of the maze to test the spontaneous turning preference of the mouse. After these two trials, the least chosen arm was reinforced by the escape platform. The mice were placed in the stem of the T-maze and were left to choose swimming either left or right until they found the submerged platform and escaped to it, for a maximum of 60 s. After reaching the platform, the mice remained on it for 20 s and were then immediately placed back into the maze. If the animals did not find the platform within this limit, they were gently guided onto it. Repeated trials were presented on the same day up to a maximum of 48 trials. A rest period of at least 10–15 min intervened between each block of 10 trials. A mouse was considered to have learned the task when it made no errors in a block of five consecutive trials. The reversal learning phase was then conducted 48 h later. During this phase, the same protocol was repeated, except that mice were trained to find the escape platform on the side opposite to where they had learned in the acquisition phase. The number of trials to reach the criterion (five of five correct choices made on consecutive trials) was measured as well as the latency to find the escape platform.

Passive avoidance test. Because the animals had a natural tendency to prefer dark environments, they were also evaluated in their retention of nonspatial memory for a one-trial passive avoidance task. The passive avoidance apparatus (Ugo Basile) was divided into two sections, one illuminated (the start compartment) and one dark (escape compartment). The floor of each compartment contained a grid, with only the dark compartment being electrified by a generator. On the training day, mice were placed into the lighted compartment for a 60-s acclimation period. The guillotine door was then opened, and the latency to enter the dark side was recorded. Immediately after entering the dark compartment, the door was closed and an electric shock (0.5 mA for 2 s) was delivered. The mouse was kept in the dark compartment for 10 s before being returned to its home cage. On the next day, the mice were placed again in the light compartment, and the step-through latency to enter the dark side was measured for up to 300 s.

Tissue Analyses

Transgenic, chimeric or lentivirus-treated mice were anesthetized under isofluorane, and blood was drawn via cardiac puncture before decapitation. Brains were rapidly removed from the skulls and placed in cold phosphate-buffered saline solution. Hemibrains were then separated and olfactory bulbs and cerebellum were removed. One hemibrain was rapidly frozen in liquid nitrogen and stored at –80°C for protein analysis. The other was postfixed for 2–4 d in 4% paraformaldehyde, pH 9.5, at 4°C and then placed in a paraformaldehyde solution containing 10% (w/v) sucrose overnight at 4°C. The frozen brains were mounted on a microtome (Reichert-Jung) and cut into 25-μm coronal sections. Slices were collected in cold cryoprotectant solution (0.05 mol/L sodium phosphate buffer, pH 7.3, 30% ethylene glycol and 20% glycerol) and stored at –20°C until performing immunocytochemistry or *in situ* hybridization histochemistry.

***In situ* hybridization and immunohistochemistry.** Every twelfth section of brain slices, starting from the end of the olfactory bulb to the end of the cerebral cortex, was mounted on Colorfrost/Plus microscope slides (Fisher Scientific, Ottawa, ON, Canada) for transgenic and chimeric mice (6 months of age, n = 5–12 per group). *In situ* hybridization for the histochemical localization of CX_3CR1, TGF-β1 and TGF-β receptors R1 and R2 was performed using ^{35}S-labeled cRNA probes. Plasmids were linearized, and sense and antisense cRNA probes were synthesized with the appropriate RNA polymerase, as described in Table 1. Riboprobe synthesis and preparation and *in situ* hybridization were performed according to a previously described protocol (40–43). For each transcript, the expression level was estimated by qualitative analysis using a Nikon Eclipse 80i microscope over the whole-brain sections for 5–10 animals/group.

Dual labeling combining immunocytochemistry and *in situ* hybridization was performed as described previously (40,42) to localize CX_3CR1 transcripts in GFP cells. We used polyclonal rabbit anti-green fluorescent protein (GFP, 1:2,000, Molecular Probes; anti-rabbit biotin-conjugated, 1:1,500, Jackson ImmunoResearch (West Grove, PA, USA).

Table 1. Plasmids and enzymes used for the synthesis of the cRNA probes.

Plasmid	Vector	Insert	Antisense probe	Sense probe	Source
Mouse CX3CR1	PCR II Topo	1132 bp	*Bam*HI/T7	*Xho*I/Sp6	Cloned by PCR
Mouse MCP-1	pGEM-1	578 bp	*Bam*HI/T7	*Sac*I/SP6	SC Williams, Texas Tech University, Lubbock, TX, USA
Mouse TGFB1 R1	PCR II Topo	1093 bp	*Not*I/Sp6	*Spe*I/T7	Cloned by PCR
Mouse TGFB1 R2	PCR II Topo	933 bp	*Xho*I/Sp6	*Bam*HI/T7	Cloned by PCR
Mouse TGFβ1	pBSKS+	1173 bp	*Eco*RI/T3	*Xho*I/T7	S Lacroix, Laval University, Québec, Canada

All images were captured using a Nikon Eclipse 80i microscope equipped with a digital camera (QImaging), processed to enhance contrast and sharpness using Adobe Photoshop 7 (Adobe Systems), and then assembled using Adobe Illustrator (Adobe Systems). The images depicted by the different panels are representative of the signal detected on the slides for each group of mice.

Stereological analysis. An observer who was blind to the treatment status of the material did all quantitative histological analyses. To count Aβ plaques and plaque-associated microglia, sections of APP_{Swe}/PS1 and APP_{Swe}/PS1/$CCR2^{-/-}$ mice or chimeric mice (6 months of age, n = 6–15 per group) were immunostained for Aβ (polyclonal mouse anti-Aβ 6E10, 1:3,000; Covance, Princeton, NJ, USA) and ionized calcium binding adaptor molecule 1 (iba-1) proteins with 4′,6′-diamidino-2-phenylindole as previously reported (7,39). Four sections were chosen for hippocampus/cerebral cortex at –1.70, –1.94, –2.46 and –2.92 mm from the bregma according to a stereotaxic atlas (44 [Paxinos and Franklin]). Unbiased stereological analysis was performed as described previously (7,39,45). Briefly, the contours of the hippocampus and the cortex areas were traced as virtual overlays on the steamed images, and areas were calculated. The area occupied by all Aβ-labeled plaques was determined as well as the plaque-associated microglia number in each structure.

Protein extraction and detection of total Aβ levels by Western blot. Proteins from hemiforebrains were extracted using a modified version of the procedure published by Lesne *et al.* (1). All manipulations were done on ice to minimize protein degradation. One hemiforebrain was placed in a 1-mL syringe with a 20-gauge needle. A total of 500 μL buffer A (50 mmol/L Tris-HCl, pH 7.6, 0.01% NP-40, 150 mmol/L NaCl, 2 mmol/L EDTA [ethylenediaminetetraacetic acid], 0.1% sodium dodecyl sulfate [SDS], 1 mmol/L phenylmethylsulfonyl fluoride [PMSF] and protease inhibitor cocktail) were added, and 10 up-and-down strokes were made to homogenize the tissue, followed by a 5-min centrifugation at 830*g* at 4°C. The supernatant (extracellular protein-enriched fraction) was then collected and frozen at –80°C. The insoluble pellet was suspended in 500 μL TNT buffer (Buffer B; 50 mmol/L Tris-HCl, pH 7.6, 150 mmol/L NaCl, 0.1% Triton X-100, 1 mmol/L PMSF and protease inhibitor cocktail), followed by a 90-min centrifugation at 15,588*g* at 4°C. The supernatant (cytoplasmic protein–enriched fraction) was then collected and frozen at –80°C. The pellet was suspended in 500 μL buffer C (50 mmol/L Tris-HCl, pH 7.4, 150 mmol/L NaCl, 0.5% Triton X-100, 1 mmol/L EGTA [ethyleneglycotetraacetic acid], 3% SDS, 1% deoxycholate, 1 mmol/L PMSF and protease inhibitor cocktail) and incubated at 4°C, 0.23*g*, for 1 h. Samples were centrifuged for 90 min at 15,588*g* at 4°C, and the supernatant (membrane protein enriched fraction) was collected and frozen at –80°C. Protein concentration of each fraction was determined using the Quantipro bicinchoninic acid assay kit (Sigma) according to the manufacturer's protocol.

For total Aβ detection, 10–20 μg extracellular, cytoplasmic and membrane protein fractions were separated on a precast 10–20% SDS polyacrylamide Tris-Tricine gel (Bio-Rad). Resolved proteins were then transferred onto polyvinylidene fluoride (PVDF) membranes (PerkinElmer, Woodbridge, ON, Canada) and detected by Western blotting. Blots were probed with a mouse anti-amyloid β protein monoclonal antibody clone 6E10 (1:1,000; Covariance) in 1 mol/L Tris-HCl, pH 8.0, 5 mol/L NaCl, 5% skim milk and 0.05% Tween 20. Blots were visualized with anti-mouse secondary antibody tagged with horseradish peroxidase (1:1,000; Jackson ImmunoResearch) using enhanced chemiluminescence (PerkinElmer). Membranes were stripped in 25 mmol/L glycine-HCl, pH 2.0, containing 1% SDS to allow β-actin revelation, first using a mouse β-actin antibody (MAB1501, 1:5,000; Millipore Bioscience Research Reagents) and then a goat anti-mouse peroxidase-conjugated secondary antibody (1:1,000; Jackson ImmunoResearch).

Quantification was done by determining the integrative density of the bands using a gel imaging system (Agfa Arcus II scanner with NIH ImageJ software, version 1.32j, for quantitation) with subtraction of background values. Optical values were normalized according to the actin loading control. Results are expressed as the mean ± standard error of the mean (SEM).

Fluorescence-Activated Cell Sorting (FACS) Analyses

Chimerism was confirmed by fluorescence-activated cell sorting (FACS) of red blood cell–lysed blood. Briefly, whole blood was taken from the facial vein and quickly suspended, and cells were washed several times in DPBS + 5% goat serum. Phycoerythrin (PE)-conjugated CD11b antibody (Cedarlane) was then added, and cells were washed again in DPBS + 5% goat serum. Red blood cells were then lysed with hemolysin according to the manu-

facturer's protocol (Beckman Coulter, Mervue, Galway, Ireland), and cells were washed with DPBS and resuspended in equal volumes of DPBS + 5% goat serum and 4% paraformaldehyde (pH 7.6). Cells were analyzed using a two-laser, four-color FACS Calibur flow cytometer and CellQuest Pro software (BD Biosciences, Mississauga, ON, Canada) and then sorted according to PE-CD11b and GFP fluorescence.

In lentiviral treatment, FACS analysis was performed on red blood cell–lysed blood. As previously described, whole blood was taken from the facial vein and was only lysed just before being analyzed by FACS to determine GFP fluorescence. To analyze the population of monocytes, anticoagulated whole blood was taken from the facial vein and quickly suspended, and cells were washed in DPBS + 4% fetal bovine serum. Cells, suspended in DPBS + 2% fetal bovine serum, were first incubated on ice for 15 min with purified rat anti-mouse CD16/CD32 (Mouse BD Fc Block, BD Biosciences). The mix was then incubated on ice with PE-Cy7–conjugated CD11b antibody (eBioscience), allophycocyanin-conjugated CD115 antibody (eBioscience), FITC Ly6-C antibody (BD Biosciences) and PerCP-Cy5.5™–conjugated Gr1 antibody (Cedarlane) for 35 min. Cells were washed again in DPBS + 2% fetal bovine serum. Red blood cells were lysed with hemolysin according to the manufacturer's protocol (Beckman Coulter, Mervue, Galway, Ireland), and cells were washed with DPBS and resuspended in equal volumes of DPBS. For CCR2 detection, washed cells were first incubated on ice with monoclonal antibody MC-21 (anti-CCR2) for 60 min (17). After washing, cells were incubated for 60 min on ice with a biotin-labeled anti-rat polyclonal antibody (BD Biosciences). Cells were washed again and incubated with purified rat anti-mouse CD16/CD32 on ice for 15 min, before adding PerCP™-labeled streptavidin antibody (BD Biosciences) and the combination of directly conjugated antibodies as described previously (17). Cells were analyzed using a two-laser and six-color FACS Canto II flow cytometer, and data acquisition was done with BD Facs Diva software (version 6.1.2, BD Biosciences). Cells were then sorted according to the respective fluorescent antibodies. Results were analyzed using Flow Jo software (Tristar).

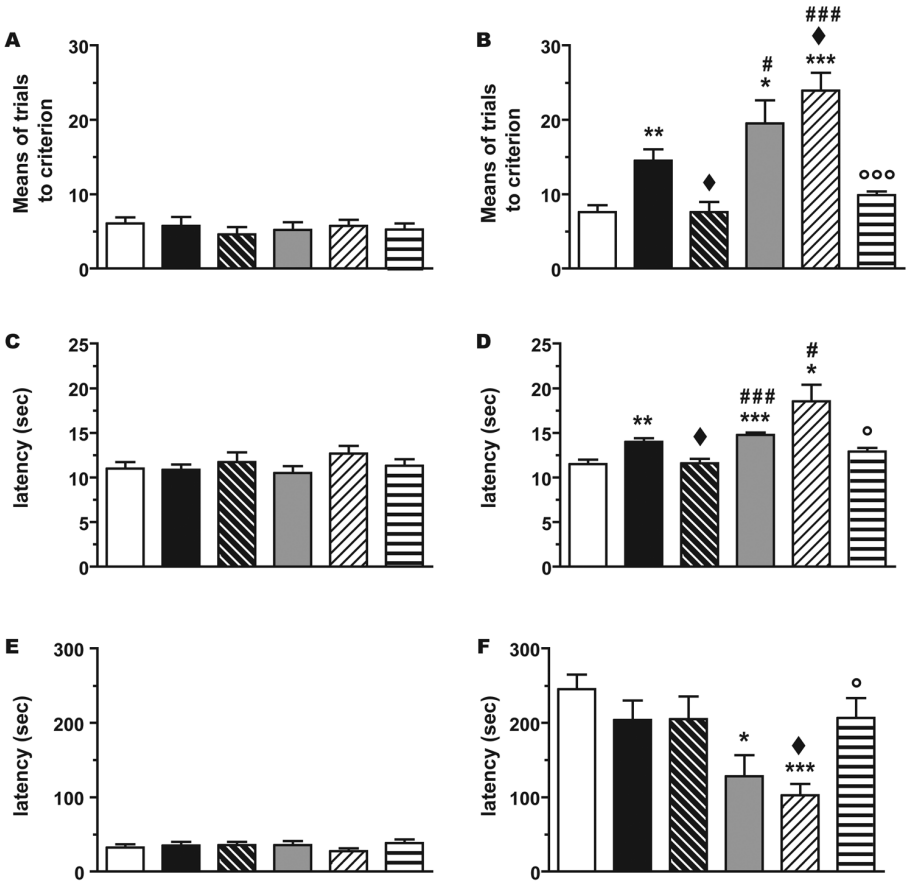

Figure 1. Spatial and contextual memory impairments are similar in APP_{Swe}/PS1 mice transplanted with CCR2-deficient BMCs and APP_{Swe}/PS1/$CCR2^{-/-}$ mice. The numbers of trials and latency to accomplish the water T-maze task were determined in mice harboring WT GFP or $CCR2^{-/-}$ cells in the bloodstream at 6 months of age for the acquisition (A, C) and reversal learning phases (B, D). The transplantation of GFP cells significantly prevented the apparition of mnesic impairment in APP_{Swe}/PS1 and APP_{Swe}/PS1/$CCR2^{-/-}$ mice. In contrast, APP_{Swe}/PS1 mice harboring $CCR2^{-/-}$ cells in their bloodstream exhibited memory impairment, comparable to that observed in APP_{Swe}/PS1/$CCR2^{-/-}$ mice. To assess contextual memory using the passive avoidance test, the latency to enter the dark box was measured during the acquisition phase (E) and 24 h after the conditioning test (F). APP_{Swe}/PS1 mice harboring $CCR2^{-/-}$ cells in their bloodstream exhibited contextual deficit similar to that of APP_{Swe}/PS1/$CCR2^{-/-}$ mice, which was rescued by the transplantation of WT GFP cells. Results are expressed as the mean ± SEM; n = 8–15; $^{*}P < 0.05$, $^{**}P < 0.01$ and $^{***}P < 0.001$ versus WT; $^{\blacklozenge}P < 0.05$ versus APP_{Swe}/PS1; $^{\#}P < 0.05$ and $^{\#\#\#}P < 0.001$ versus GFP → APP_{Swe}/PS1; $^{\circ}P < 0.05$ and $^{\circ\circ\circ}P < 0.001$ versus APP_{Swe}/PS1/$CCR2^{-/-}$. One-way ANOVA was performed using a Tamhane *post hoc* test. □, WT; ■, APP_{Swe}/PS1; ⬕, GFP → APP_{Swe}/PS1; ▩, $CCR2^{-/-}$ → APP_{Swe}/PS1; ▨, APP_{Swe}/PS1/$CCR2^{-/-}$; ▤, GFP → APP_{Swe}/PS1/$CCR2^{-/-}$.

Statistical Analyses

Results are expressed as the mean ± SEM. Statistical analysis was performed by one- or two-way analysis of variance (ANOVA), followed by the appropriate test procedure, using Bonferroni, Dunnett or Tamhane tests as *post hoc* comparisons

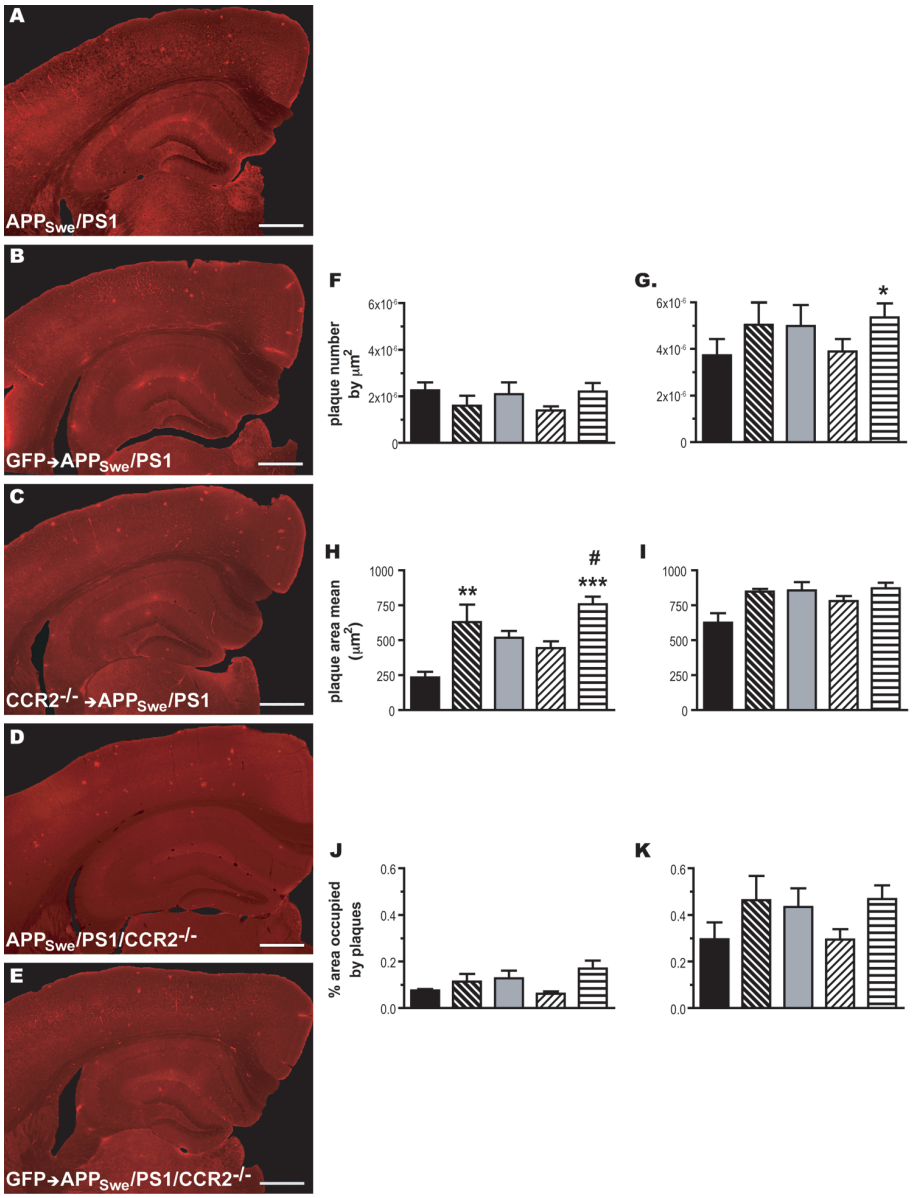

Figure 2. Aβ plaque formation remains similar in the brain of APP_{Swe}/PS1 and APP_{Swe}/PS1/$CCR2^{-/-}$ mice transplanted with WT (GFP) or $CCR2^{-/-}$ BMCs. Hemibrain sections of 6-month-old APP_{Swe}/PS1 and APP_{Swe}/PS1/$CCR2^{-/-}$ mice transplanted with GFP or $CCR2^{-/-}$ BMC (A–E) were immunostained for Aβ. Stereological analysis was performed to determine plaque density (F–G), plaque size (H–I) and the percentage area occupied by plaques (J–K) for each group in the hippocampus (F, H, J) and cerebral cortex (G, I, K). Transplantation of GFP or $CCR2^{-/-}$ cells in APP_{Swe}/PS1 and APP_{Swe}/PS1/$CCR2^{-/-}$ mice had no major effect on plaque formation. Results are expressed as the mean ± SEM; n = 6–15; $^{*}P < 0.05$, $^{**}P < 0.01$ and $^{***}P < 0.001$ versus APP_{Swe}/PS1; $^{\#}P < 0.05$ versus APP_{Swe}/PS1/$CCR2^{-/-}$. One-way ANOVA was performed using the Bonferroni or Tamhane *post hoc* test. Scale bar 500 µm. ■, APP_{Swe}/PS1; ◪, GFP → APP_{Swe}/PS1; ▩, $CCR2^{-/-}$ → APP_{Swe}/PS1; ◩, APP_{Swe}/PS1/$CCR2^{-/-}$; ▤, GFP → APP_{Swe}/PS1/$CCR2^{-/-}$.

(SPSS software). Data were analyzed using standard two-tailed unpaired *t* tests for the comparison between two groups. The relationship between spatial working memory and levels of soluble Aβ species (extracellular- or membrane-associated proteins) were determined in two groups of animals. The first group was composed of APP_{Swe}/PS1, WT (GFP) → APP_{Swe}/PS1 and $CCR2^{-/-}$ → APP_{Swe}/PS1 mice. The second group contained APP_{Swe}/PS1/$CCR2^{-/-}$ and WT (GFP) → APPSwe/PS1/$CCR2^{-/-}$ mice. Correlations were estimated by linear regression analysis and the Spearman correlation coefficient (GraphPad Software) with *P* and *r* values and 95% confidence intervals are included in the graph. $P < 0.05$ was considered statistically significant.

RESULTS

CCR2 Deficiency in BMCs Exacerbates Cognitive Decline in APP_{Swe}/PS1 Mice

To establish whether CCR2 deficiency in resident or bone marrow–derived microglia is responsible for exacerbating the pathology in this mouse model of AD, we generated APP_{Swe}/PS1 and APP_{Swe}/PS1/$CCR2^{-/-}$ mice harboring WT GFP or $CCR2^{-/-}$ BMC; all mice exhibited a high level of chimerism (~93%, data not shown). Learning and contextual memory were assessed using water T-maze and passive avoidance tests. For both tests, all different mouse groups exhibited similar learning capacity during the acquisition phase (Figures 1A, C, E). During the reversal learning phase of the water T-maze test, transplantation with GFP-expressing BMCs rescued spatial memory in APP_{Swe}/PS1 and APP_{Swe}/PS1/$CCR2^{-/-}$ mice, as evidenced by the decreased number of trials (7.6 ± 1.4 versus 14.5 ± 1.5 for APP_{Swe}/PS1, $P < 0.05$, and 9.8 ± 0.5 versus 23.9 ± 2.4 for APP_{Swe}/PS1/$CCR2^{-/-}$, $P < 0.001$) (Figure 1B) and latency (11.6 ± 0.5 versus 14.0 ± 1.4 for APP_{Swe}/PS1, $P < 0.05$, and 12.9 ± 0.4 versus 18.5 ± 1.8 for APP_{Swe}/PS1/$CCR2^{-/-}$, $P < 0.05$) (Figure 1D). In contrast, memory impairment were similarly aggravated in APP_{Swe}/PS1 mice transplanted with $CCR2^{-/-}$ BMCs and APP_{Swe}/PS1/$CCR2^{-/-}$ mice, as shown by the number of trials (19.6 ± 3.1 versus 23.9 ± 2.4 for APP_{Swe}/PS1/$CCR2^{-/-}$) (Figure 1B) and latency (14.8 ± 0.5 versus 18.5 ± 1.8 for APP_{Swe}/PS1/$CCR2^{-/-}$) (Fig-

ure 1D). During a passive avoidance test, transplantation of GFP cells also rescued contextual memory impairment in $APP_{Swe}/PS1/CCR2^{-/-}$ mice (206 ± 27 versus 103 ± 15 in $APP_{Swe}/PS1/CCR2^{-/-}$; $P < 0.05$) 24 h after the conditioning test. In contrast, $APP_{Swe}/PS1$ mice transplanted with $CCR2^{-/-}$ BMCs exhibited a deficit of contextual memory similar to that seen in $APP_{Swe}/PS1/CCR2^{-/-}$ mice (128 ± 28 for $CCR2^{-/-} \rightarrow APP_{Swe}/PS1$ and 103 ± 15 for $APP_{Swe}/PS1/CCR2^{-/-}$ versus 204 ± 26 in $APP_{Swe}/PS1$; $P < 0.05$ and $P < 0.001$, respectively) (Figure 1F). Taken together, these data demonstrate that CCR2 deficiency specifically in HSCs aggravates spatial and contextual impairment in this mouse model of AD.

Transplantation of WT (GFP) or $CCR2^{-/-}$ BMCs Does Not Modify the Formation of Aβ Deposits, But Does Induce Changes in Soluble Aβ Oligomer Levels

Despite an increase of plaque size in the hippocampus of $APP_{Swe}/PS1$ and $APP_{Swe}/PS1/CCR2^{-/-}$ mice that were transplanted with GFP cells (630 ± 125 versus 234 ± 41 μm^2 in $APP_{Swe}/PS1$ and 757 ± 55 versus 444 ± 47 μm^2 in $APP_{Swe}/PS1/CCR2^{-/-}$; $P < 0.01$ and $P < 0.05$, respectively) (Figure 2H), plaque density and the percentage of area occupied by plaques in hippocampus and cortex remained similar in $APP_{Swe}/PS1$ or $APP_{Swe}/PS1/CCR2^{-/-}$ mice harboring WT GFP or $CCR2^{-/-}$ BMCs (Figure 2). Therefore, no correlation was observed between mnesic deficit and Aβ plaque burden. As reported in the literature, memory deficits correlate more strongly with cortical levels of soluble Aβ species than with insoluble Aβ plaque burden in AD patients (46,47) and mouse models of AD (1,48).

Western blots revealed a decrease of soluble extracellular Aβ oligomers of low molecular mass (6-, 3-, 2- and 1-mer) in the brain of $APP_{Swe}/PS1$ and $APP_{Swe}/PS1/CCR2^{-/-}$ mice transplanted with WT GFP cells, whereas $APP_{Swe}/PS1$ mice transplanted with $CCR2^{-/-}$ BMCs exhibited enhanced levels of soluble extracellular Aβ oligomers, comparable to soluble

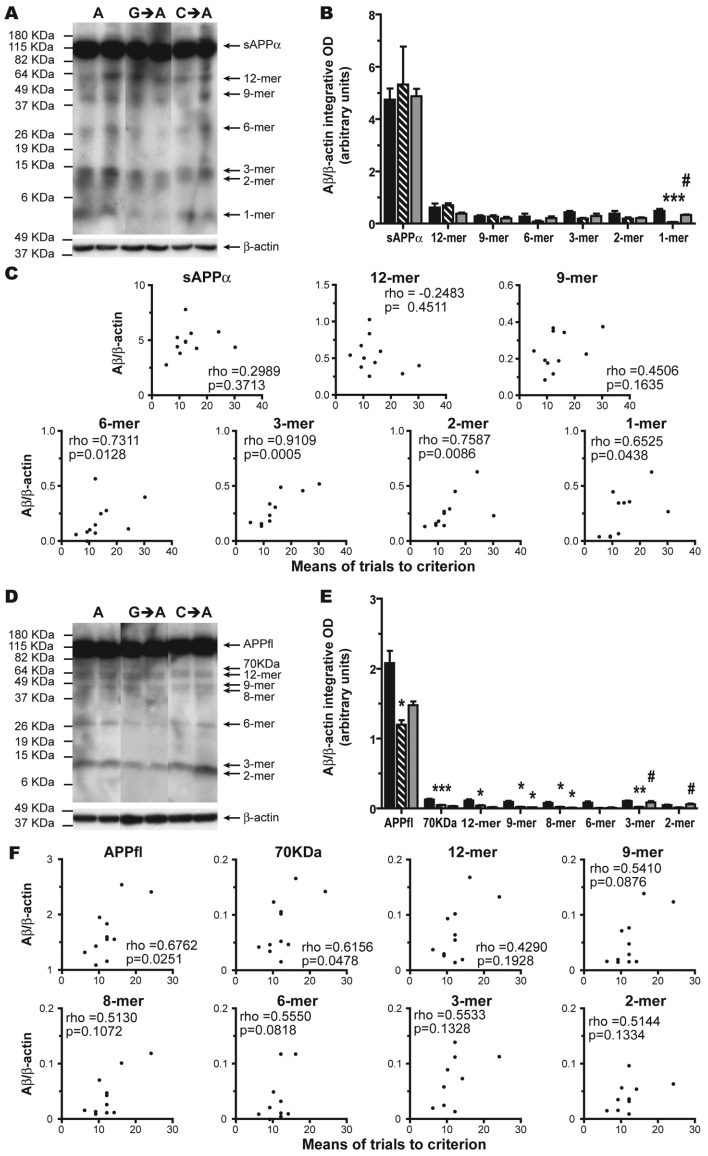

Figure 3. $APP_{Swe}/PS1$ mice harboring WT (GFP) BMCs exhibit decreased levels of soluble extracellular and membrane-associated Aβ species, which are increased in $APP_{Swe}/PS1$ mice after transplantation of $CCR2^{-/-}$ cells. Hemibrain extracts from soluble extracellular (A) and membrane-associated proteins (D) of 6-month-old $APP_{Swe}/PS1$ mice harboring WT GFP or $CCR2^{-/-}$ cells in their bone marrow were assessed by Western blot on a 10–20% Tris-Tricine denaturing polyacrylamide gel to separate Aβ species using anti-Aβ antibody 6E10. The intensity of each band was quantified by densitometric analysis and normalized to β-actin values. Each Aβ species ratio (Aβ/β-actin) is represented for extracellular (B) and membrane-associated proteins (E). Lower levels of soluble extracellular and membrane-associated Aβ species were found in mice harboring WT BMCs, whereas Aβ oligomer levels increased in mice transplanted with CCR2-deficient BMCs. Correlations were determined between spatial memory decline (water T-maze test) and soluble Aβ species in extracellular (C) and membrane-associated (F) fractions. Results are expressed as the mean ± SEM; n = 4–5; $^{*}P < 0.05$, $^{**}P < 0.01$ and *** $P < 0.001$ versus $APP_{Swe}/PS1$; $^{\#}P < 0.05$ versus GFP → $APP_{Swe}/PS1$. One-way ANOVA was performed using Dunnett or Tamhane *post hoc* tests; for the Dunnett test, the control group was GFP → $APP_{Swe}/PS1$ mice. Correlation was estimated by the Spearman correlation coefficient. OD, optical density; ■, $APP_{Swe}/PS1$; ◪, GFP → $APP_{Swe}/PS1$; ▩, $CCR2^{-/-}$ → $APP_{Swe}/PS1$.

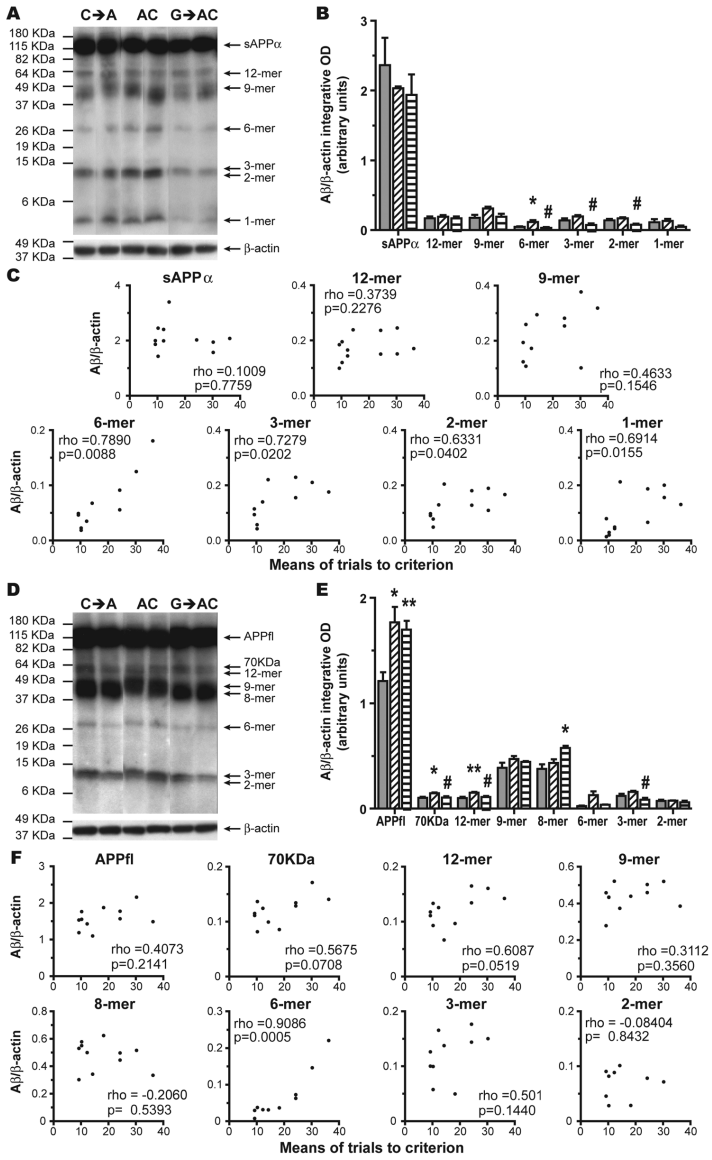

Figure 4. Soluble extracellular and membrane-associated Aβ species levels in the brain of $APP_{Swe}/PS1/CCR2^{-/-}$ mice transplanted with WT (GFP) BMCs. Hemibrain extracts from soluble extracellular (A and D) and membrane-associated proteins (G and J) of 6-month-old $APP_{Swe}/PS1/CCR2^{-/-}$ mice harboring WT (GFP) BMCs were assessed by Western blot on a 10–20% Tris-Tricine denaturing polyacrylamide gel to separate Aβ species using anti-Aβ antibody 6E10. The intensity of each band was quantified by densitometric analysis and normalized to β-actin values. Ratios of Aβ species (Aβ/β-actin) are represented for extracellular (B) and membrane-associated proteins (E). Lower levels of soluble extracellular and membrane-associated Aβ species were found in mice harboring WT BMCs, whereas Aβ oligomer levels increased in mice transplanted with CCR2-deficient BMCs. Correlations were determined between spatial memory decline (water T-maze test) and soluble Aβ species in extracellular (C) and membrane-associated (F) fractions. Results are expressed as the mean ± SEM; n = 4–5; $^{*}P < 0.05$ and $^{**}P < 0.01$ versus $CCR2^{-/-} \rightarrow APP_{Swe}/PS1$; $^{\#}P < 0.05$ versus $APP_{Swe}/PS1/CCR2^{-/-}$. One-way ANOVA was performed using Dunnett or Tamhane *post hoc* tests; for the Dunnett test the control group was $APP_{Swe}/PS1/CCR2^{-/-}$ mice. Correlation was estimated by the Spearman correlation coefficient. OD, optical density; ■, $CCR2^{-/-} \rightarrow APP_{Swe}/PS1$; ▨, $APP_{Swe}/PS1/CCR2^{-/-}$; ▤, GFP → $APP_{Swe}/PS1/CCR2^{-/-}$.

Aβ levels of $APP_{Swe}/PS1/CCR2^{-/-}$ mice (Figures 3A, B, and 4A, B, respectively). A positive and strong correlation was shown between memory deficit and the levels of extracellular low–molecular mass oligomers (Figures 3C, 4C). Similarly, WT GFP BMC transplantation reduced membrane-associated Aβ levels, particularly the 3-mer (Figures 3D, E, and 4D, E, respectively), whereas $CCR2^{-/-}$ cell transplantation in $APP_{Swe}/PS1$ mice caused an increase of 2- and 3-mer levels compared with the control group GFP → $APP_{Swe}/PS1$ mice (Figures 3D, E). However, no correlation was found between cognitive deficit and Aβ oligomers associated with membrane, except for full-length APP (APPfl) (Figure 3F). Transplantation of GFP or $CCR2^{-/-}$ cells had no effect on soluble intracellular Aβ oligomers in $APP_{Swe}/PS1$ and $APP_{Swe}/PS1/CCR2^{-/-}$ mice (Figure 5). In conclusion, competent CCR2 HSCs are able to control Aβ production and/or clearance.

Cytokine Gene Expression in the Brain of AD Mice Bearing CCR2-Deficient BMCs

As previously observed (39), expression of TGF-β1, TGF-β-R1 and TGF-β-R2 mRNA increased in the brain of 6-month-old $APP_{Swe}/PS1$ mice (Figures 6A, E, I, M). Transplantation of WT GFP BMCs strongly diminished TGF-β1 and TGF-β receptor expression by plaque-associated microglia in $APP_{Swe}/PS1$ (Figures 6B, F, J, M) and $APP_{Swe}/PS1/CCR2^{-/-}$ mice (Figures 6D, H, L, M). In contrast, TGF-β1, TGF-β-R1 and TGF-β-R2 mRNA signal increased in microglia surrounding senile plaques of $APP_{Swe}/PS1$ mice harboring $CCR2^{-/-}$ BMCs when compared with control GFP → $APP_{Swe}/PS1$ mice (Figures 6C, G, K, M). Stereological analysis revealed an increase of the number of microglia associated with Aβ deposits in the hippocampus of $APP_{Swe}/PS1/CCR2^{-/-}$ mice compared with the other groups (Figure 7F). In contrast, transplantation of GFP cells significantly reduced microglia recruitment around Aβ plaques in hippocampus (see Figure 7F) and cortex (Figure 7G) of $APP_{Swe}/PS1/CCR2^{-/-}$ mice

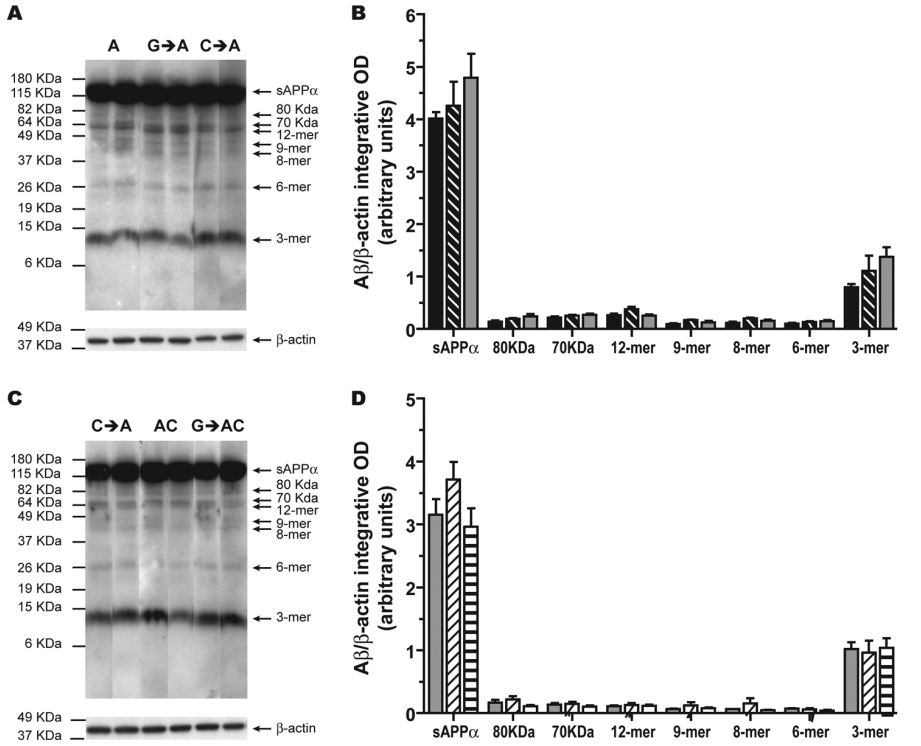

Figure 5. Similar soluble intracellular Aβ species in the brain of APP_{Swe}/PS1 and APP_{Swe}/PS1/$CCR2^{-/-}$ mice transplanted with WT (GFP) or $CCR2^{-/-}$ BMCs. Hemibrain extracts from soluble intracellular proteins (A, C) of 6-month-old APP_{Swe}/PS1 and APP_{Swe}/PS1/$CCR2^{-/-}$ mice harboring WT GFP or $CCR2^{-/-}$ cells in their bone marrow were assessed by Western blot. Densitometric analysis was used to measure the intensity of each band, which was normalized to β-actin corresponding values. Each Aβ species ratio (Aβ/β-actin) was represented for intracellular proteins (B, D). All groups of mice had similar soluble intracellular Aβ species levels. Results are expressed as the mean ± SEM; n = 4–5. One-way ANOVA was performed using Dunnett or Tamhane *post hoc* tests. OD, optical density; ■, APP_{Swe}/PS1; ◪, GFP → APP_{Swe}/PS1; ▨, $CCR2^{-/-}$ → APP_{Swe}/PS1; ▨, APP_{Swe}/PS1/$CCR2^{-/-}$; ▤, GFP → APP_{Swe}/PS1/$CCR2^{-/-}$.

and in cortex of APP_{Swe}/PS1 mice (Figure 7G). APP_{Swe}/PS1 mice transplanted with $CCR2^{-/-}$ BMCs had similar recruitment of microglia as APP_{Swe}/PS1 mice transplanted with WT BMCs. The enhanced expression of MCP-1 observed in APP_{Swe}/PS1 mice is not affected by WT BMC transplantation but is increased by transplantation of CCR2-deficient BMCs (Figures 7C, E). The enhanced expression of MCP-1 previously observed in APP_{Swe}/PS1/$CCR2^{-/-}$ mice did not occur in APP_{Swe}/PS1/$CCR2^{-/-}$ mice transplanted with WT BMCs. Microglia recruitment did not correlate with MCP-1 or CCR2 expression. These data raised questions about the origin of these recruited cells in the plaque vicinity, since these cells may derive from local and/or systemic progenitors (7). To determine the proportion of each monocyte subset recruited into brain, the CX_3CR1 level was assessed in brain GFP cells of APP_{Swe}/PS1 and APP_{Swe}/PS1/$CCR2^{-/-}$ mice transplanted with GFP BMCs. High and low levels of CX_3CR1 transcripts was observed in GFP cells in the brain of both groups of mice (Figures 7I, J). These data suggest that a strong brain recruitment of the two monocyte subsets (for example, $CX_3CR1^{high}CCR2^{-}Gr1^{-}$ and CX_3CR1^{low}-$CCR2^{+}Gr1^{+}$) occurs in a context of AD.

Thus, APP_{Swe}/PS1 mice harboring WT or CCR2-deficient BMCs exhibited similar recruitment of microglia around Aβ plaques, which exhibited different phenotypes.

Monocyte Frequency Changes in $CCR2^{-/-}$, APP_{Swe}/PS1/$CCR2^{-/-}$ and APP_{Swe}/PS1 Mice Transplanted with $CCR2^{-/-}$ BMCs

To assess whether transplantation of BMCs influences leukocyte levels, monocyte frequency and the distribution of the Gr1 status in the population was determined by FACS analysis. Interestingly, monocyte frequency was significantly higher in mice that were transplanted with WT BMCs than in mice receiving CCR2-deficient cells (Figure 8). The decrease of monocyte frequency was similar in APP_{Swe}/PS1 mice transplanted with $CCR2^{-/-}$ BMCs and in $CCR2^{-/-}$ and APP_{Swe}/PS1/$CCR2^{-/-}$ mice. Moreover, APP_{Swe}/PS1 mice harboring WT BMCs had more $CD11b^{+}$ $CD115^{+}$ cells than APP_{Swe}/PS1 mice harboring $CCR2^{-/-}$ BMCs (6.17 ± 0.71% versus 1.13 ± 0.08% of leukocytes in APP_{Swe}/PS1 mice harboring $CCR2^{-/-}$ BMCs; $P < 0.001$, Figures 8A, B). $Gr1^{+}$ monocytes were also increased (4.06 ± 0.81% versus 0.30 ± 0.04% of leukocytes in APP_{Swe}/PS1 mice harboring $CCR2^{-/-}$ BMCs; Figures 8C, D) and the ratio of $Gr1^{+}/Gr1^{-}$ monocytes remained higher in APP_{Swe}/PS1 mice harboring WT BMCs (2.13 ± 0.60 versus 0.37 ± 0.04 in APP_{Swe}/PS1 mice harboring $CCR2^{-/-}$ BMCs; Figures 8C, D). To resume, transplanted mice acquired the hematopoietic system of the donor. Therefore, transplantation of WT BMCs attributed a WT monocyte frequency with a greater proportion of the $Gr1^{+}$ subset.

Lenti-GFP-CCR2 Rescues Memory Impairments in APP_{Swe}/PS1 and APP_{Swe}/PS1/$CCR2^{-/-}$ Mice and Increases CCR2 Expression and the Number of Circulating $CCR2^{+}$ Monocytes in $CCR2^{-/-}$ Mice

To further investigate the role of the CCR2-competent BMCs, we injected lenti-GFP-CCR2 or its control lenti-GFP in the femoral cavity of nonirradiated APP_{Swe}/PS1 and APP_{Swe}/PS1/$CCR2^{-/-}$ mice. Three

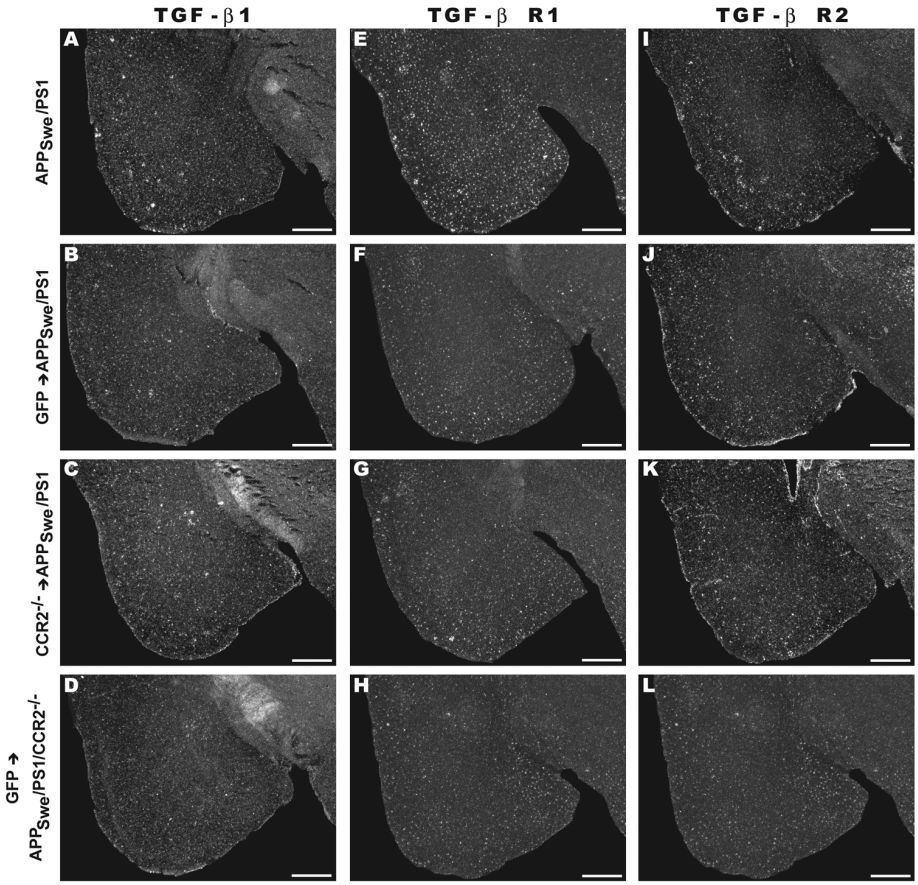

M

mRNA	APP_{Swe}/PS1	GFP → APP_{Swe}/PS1	$CCR2^{-/-}$ → APP_{Swe}/PS1	GFP → APP_{Swe}/PS1/$CCR2^{-/-}$
TGF-β1	+++	+	++	+
TGF-β R1	+++	+	++	+
TGF-β R2	+++	+	++	+

Figure 6. Expression of TGF-β1, and of TGF-β-R1 and -R2, mRNA in the brain of APP_{Swe}/PS1 mice transplanted with WT (GFP) or CCR2-deficient BMCs. Representative dark-field photomicrographs of *in situ* hybridization are shown of the cortical expression of TGF-β1 (left panels), TGF-β-R1 (middle panels) and TGF-β-R2 mRNA (right panels) in 6-month-old APP_{Swe}/PS1 and APP_{Swe}/PS1/$CCR2^{-/-}$ harboring bone marrow GFP or $CCR2^{-/-}$ cells. Qualitative quantification was performed for each transcript (n = 5–12) (M). A decrease in TGF-β1, and in TGF-β-R1 and -R2, mRNA levels was found in the brain of mice transplanted with WT GFP cells. Scale bar 500 μm. M: The plus signs correspond to the intensity and the surface of the signal. The number of the plus signs shows augment proportionally with the intensity and the surface.

months later, lenti-GFP-CCR2–treated mice exhibited a significant improvement of their spatial learning memory during the water T-maze test (Figures 9B, D). Interestingly, CCR2 overexpression in BMCs of the APP_{Swe}/PS1 also prevented the apparition of the spatial learning deficit. FACS analyses revealed that GFP protein is expressed by <1% leukocytes at 2 months and almost 2% at 3 months after femoral injections (Figure 9E). Detailed analysis of leukocyte population provided evidence that monocytes preferentially expressed the lentiviral construction with the CCR2 transgene (see Figure 9E). More importantly, CCR2-GFP microglia were found in the vicinity of senile plaques in the hippocampus (Figure 9H) and cerebral cortex of nonirradiated APP_{Swe}/PS1/$CCR2^{-/-}$ mice (Figures 9F, G).

A detailed analysis of the monocytic population showed that intrafemorally injected lenti-GFP-CCR2 increased CCR2 expression in monocytes of $CCR2^{-/-}$ mice (2.08 ± 0.06% versus 1.25 ± 0.21% of monocytes in lenti-GFP–injected $CCR2^{-/-}$ mice; $P < 0.05$, Figure 10H). Four weeks after intrafemoral injection, CCR2 was expressed in the circulating $CD11b^+CD115^+$Ly6-C^+ monocyte subset of $CCR2^{-/-}$ mice. The specificity of the signal was verified by FACS in WT and $CCR2^{-/-}$ mice, and $CCR2^+$ cells were detected only in the bloodstream of WT mice (data not shown). CCR2 plays a critical role in monocyte emigration from bone marrow (22), particularly for the Ly6-C^{high} (21) or $Gr1^+$ cell subsets (20). The weak frequency of these monocyte subsets in the bloodstream of $CCR2^{-/-}$ mice was efficiently restored by lenti-GFP-CCR2 treatment. Indeed, the frequency of $CD11b^+CD115^+$ monocytes (1.13 ± 0.11% versus 0.49 ± 0.19% of leukocytes in lenti-GFP-injected $CCR2^{-/-}$ mice; $P < 0.05$, Figures 11A–D) and, more specifically, the Ly6-C^{high} subset (0.249 ± 0.030% versus 0.114 ± 0.032% of leukocytes in lenti-GFP-injected $CCR2^{-/-}$ mice; $P < 0.05$, Figures 11E–H) or $Gr1^+$ subset (0.281 ± 0.024% versus 0.145 ± 0.023% of leukocytes in lenti-GFP–injected $CCR2^{-/-}$ mice; $P < 0.05$, Figures 11I–L) were increased after lenti-GFP-CCR2 injection in $CCR2^{-/-}$ mice. These data, together with higher frequencies of $CD11b^+CD115^+Gr1^-$ monocytes (0.780 ± 0.099% versus 0.304 ± 0.160% of leukocytes in lenti-GFP–injected $CCR2^{-/-}$ mice; $P < 0.05$, Figures 11I–L) suggest that the comparatively small population of CCR2-expressing cells is able to emigrate from the bone marrow and rescue cognitive deficit in a context of CCR2 deficiency.

DISCUSSION

We previously demonstrated that CCR2 deficiency in a mouse model of AD accelerates disease onset and aggravates mnesic deficits (37). Here we show that transplantation of CCR2-deficient BMCs

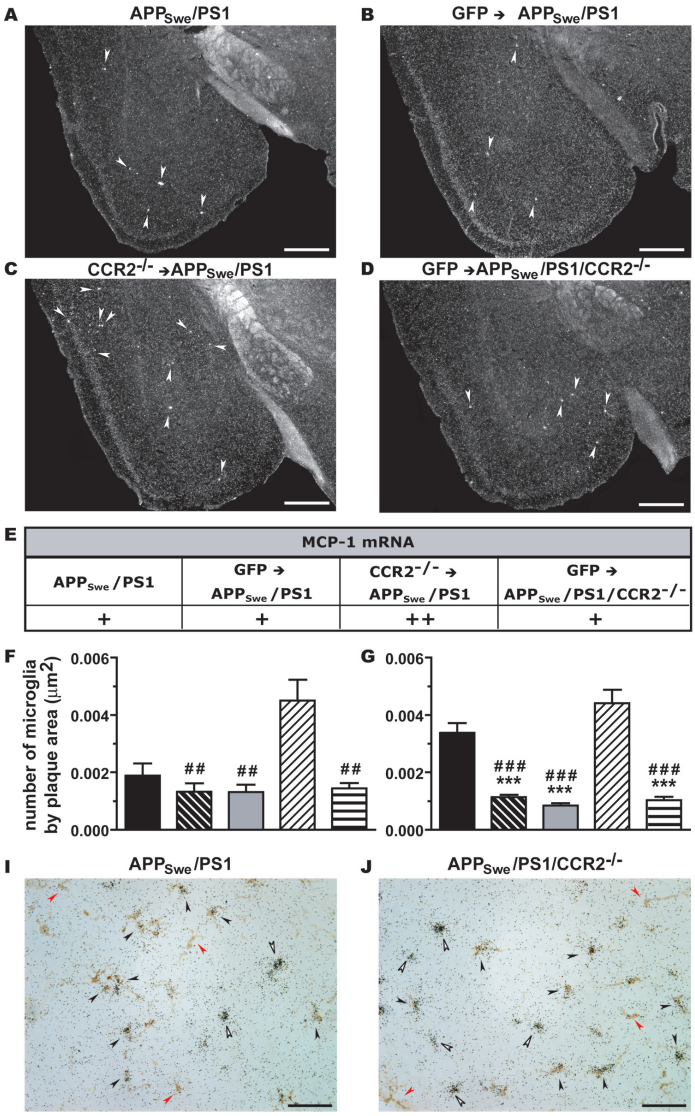

Figure 7. CCR2-deficient BMCs increase MCP-1 expression in APP_{Swe}/PS1 mice. Representative dark-field photomicrographs of *in situ* hybridization showing the cortical expression of MCP-1 in the brains of 6-month-old APP_{Swe}/PS1 and APP_{Swe}/PS1/$CCR2^{-/-}$ mice harboring GFP or $CCR2^{-/-}$ BMC (A–D). MCP-1 qualitative quantification was performed for each group of mice (n = 5–12) (E). Transplantation of $CCR2^{-/-}$ cells caused an increase in the MCP-1 transcript levels. Brain sections were immunostained for Aβ and iba-1, and the number of plaque-associated microglia was determined in hippocampus (F) and cortex (G). APP_{Swe}/PS1 and APP_{Swe}/PS1/$CCR2^{-/-}$ harboring GFP or $CCR2^{-/-}$ BMC exhibited less recruitment of microglia in the plaque vicinity. Brain sections of APP_{Swe}/PS1 (I) and APP_{Swe}/PS1/$CCR2^{-/-}$ (J) mice harboring GFP-expressing cells in their bloodstream were labeled to reveal GFP cells (brown cells) together with CX_3CR1 mRNA (silver grains). Results are expressed as the mean ± SEM; n = 8–16; $^{***}P < 0.001$ versus APP_{Swe}/PS1; $^{\#\#}P < 0.01$ and $^{\#\#\#}P < 0.001$ versus APP_{Swe}/PS1/$CCR2^{-/-}$. One-way ANOVA was performed using Bonferroni or Tamhane *post hoc* tests. A–D: Arrowheads: MCP-1 positive signal; I and J: black arrowheads: double-labeled cells (GFP/CX_3CR1 mRNA); open arrowheads: CX_3CR1-positive cells (negative for GFP); red arrowheads: GFP-positive cells (negative for CX_3CR1 mRNA). Scale bar 500 μm (A–D) and 50 μm (I and J). E: The plus signs correspond to the intensity and the surface of the signal. The number of the plus signs shows augment proportionally with the intensity and the surface. ■, APP_{Swe}/PS1; ◪, GFP → APP_{Swe}/PS1; ▩, $CCR2^{-/-}$ → APP_{Swe}/PS1; ▨, APP_{Swe}/PS1/$CCR2^{-/-}$; ▤, GFP → APP_{Swe}/PS1/$CCR2^{-/-}$.

in APP_{Swe}/PS1 mice causes similar effects: APP_{Swe}/PS1/$CCR2^{-/-}$ mice and APP_{Swe}/PS1 mice harboring CCR2-deficient BMCs exhibit significant spatial and contextual memory impairments. Moreover, cognitive capacities are restored in APP_{Swe}/PS1 and APP_{Swe}/PS1/$CCR2^{-/-}$ mice after transplantation of WT GFP BMCs or the expression of lentivirus-induced CCR2 in the bone marrow. It is important to note that APP_{Swe}/PS1/$CCR2^{-/-}$ mice already exhibited mnesic impairments and increased levels of soluble Aβ at the age of transplantation (2.5–3 months). Such defects are normally detected only at 6 months of age in APP_{Swe}/PS1 mice, suggesting that transplantation of WT BMCs does not only prevent the onset of the disease, but also cures the pathology in this mouse model of AD. These data provide solid evidence of the beneficial effect of CCR2-expressing BMCs in AD. Moreover, the rescue of mnesic capacity by WT BMC transplantation in APP_{Swe}/PS1 mice suggests a defect of hematopoietic system in a context of APP production. The ability of an intrafemoral injection of lenti-CCR2 to restore the cognitive capacity of APP_{Swe}/PS1 mice further supports an impairment of CCR2 expression/function in the BMCs of these mice.

In AD brains, Aβ can accumulate as both soluble and insoluble assemblies, and the correlation between parenchymal Aβ deposits (that is, insoluble Aβ) and the degree of cognitive impairment is no longer supported by strong evidence. Levels of smaller soluble Aβ oligomers correlate more strongly with memory decline in the brains of both AD patients (46,47) and mouse models of AD (1,48,50). In the present study, transplantation of WT or $CCR2^{-/-}$ BMCs in APP_{Swe}/PS1 and APP_{Swe}/PS1/$CCR2^{-/-}$ mice had no effect on Aβ deposition when compared with control littermates. In contrast, transplantation of WT BMCs reduced the levels of small Aβ oligomers (6-, 3-, 2- and 1-mers) in extracellular- and membrane-associated proteins, concomitantly with a rescue of mnesic deficits in both groups of APP_{Swe}/PS1 and APP_{Swe}/PS1/$CCR2^{-/-}$ chimeric

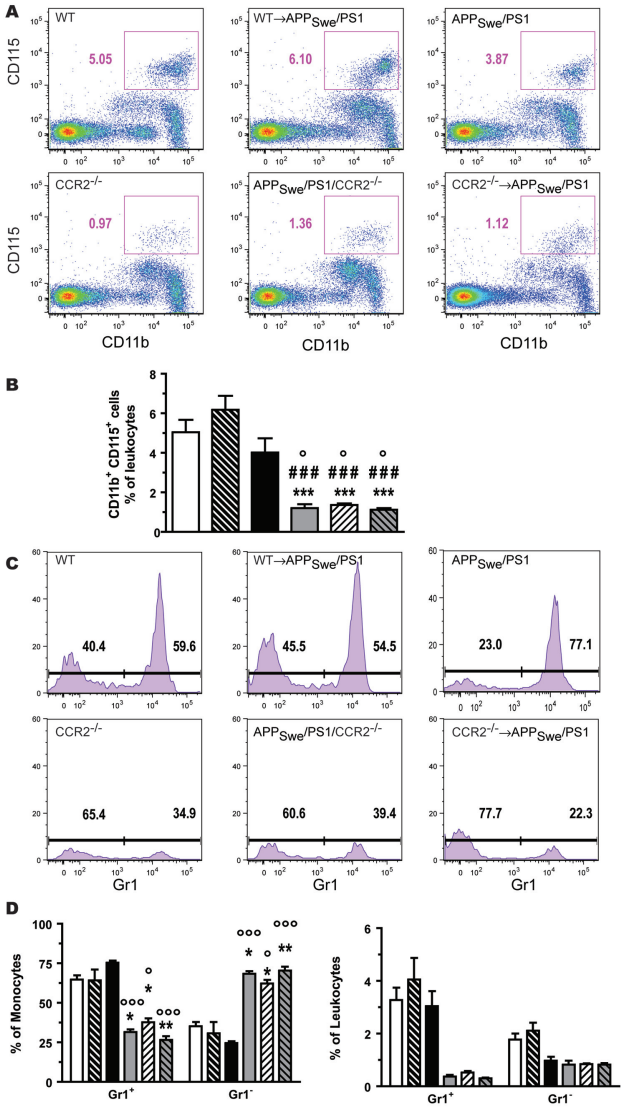

Figure 8. CCR2$^{-/-}$ BMC transplantation in APP$_{Swe}$/PS1 mice reduces monocyte frequencies and inverses the ratio of Gr1^{+}/Gr1^{-} monocytes, as observed in CCR2$^{-/-}$ and APP$_{Swe}$/PS1/CCR2$^{-/-}$ mice. Whole blood was taken and stained with fluorescent antibodies for CD11b, CD115 and Gr1 and analyzed by FACS in 4-month-old WT, CCR2$^{-/-}$, APP$_{Swe}$/PS1/CCR2$^{-/-}$ mice and APP$_{Swe}$/PS1 mice harboring WT or CCR2$^{-/-}$ BMCs. Monocytes were characterized by CD11b and CD115 expression (A). Percentages of monocytes in leukocytes were quantified (B). Gr1 expression was assessed in monocytes. The percentage of Gr1^{+} or Gr1^{-} monocytes was determined in monocytes and in leukocytes (D). Monocyte frequencies were drastically decreased in CCR2$^{-/-}$, APP$_{Swe}$/PS1/CCR2$^{-/-}$ mice and APP$_{Swe}$/PS1 mice harboring CCR2$^{-/-}$ BMCs. In contrast, APP$_{Swe}$/PS1 mice harboring WT BMCs had higher level of monocytes, as observed in WT and APP$_{Swe}$/PS1 mice. CCR2$^{-/-}$, APP$_{Swe}$/PS1/CCR2$^{-/-}$ mice and APP$_{Swe}$/PS1 mice harboring CCR2$^{-/-}$ BMCs exhibited similarly decreased levels of Gr1^{+} and Gr1^{-} monocytes. Each graph shows a representative example of each group. Numbers near boxes indicate the percentage of CD11b^{+} CD115^{+} cells (A) and Gr1^{+} or Gr1^{-} monocytes (C) for this example. Results are expressed as the mean ± SEM; n = 3–4; $^{*}P < 0.05$, $^{**}P < 0.01$ and $^{***}P < 0.001$ versus WT mice; $^{###}P < 0.001$ versus WT → APP$_{Swe}$/PS1 mice; $^{°}P < 0.05$ and $^{°°°}P < 0.001$ versus APP$_{Swe}$/PS1 mice. One-way ANOVA using Bonferroni or Tamhane *post hoc* tests was performed. □, WT; ◪, WT → APP$_{Swe}$/PS1; ■, APP$_{Swe}$/PS1; ▩, CCR2$^{-/-}$; ▨, APP$_{Swe}$/PS1/CCR2$^{-/-}$; ◪, CCR2$^{-/-}$ → APP$_{Swe}$/PS1.

mice. Conversely, transplantation of CCR2$^{-/-}$ cells aggravated cognitive deficits in APP$_{Swe}$/PS1 mice and induced higher levels of Aβ oligomers in extracellular-enriched and membrane-associated fractions. In addition, levels of small Aβ oligomers (6-, 3-, 2- and 1-mers) in extracellular proteins strongly correlated with the degree of mnesic impairments. Of interest, Aβ dimer and trimer levels in the membrane-associated protein fraction decreased in APP$_{Swe}$/PS1 and APP$_{Swe}$/PS1/CCR2$^{-/-}$ mice transplanted with WT BMCs, whereas they increased in APP$_{Swe}$/PS1 mice transplanted with CCR2$^{-/-}$ BMCs. These small soluble oligomers can disrupt learning behavior (51), are toxic for neurons and disrupt synaptic plasticity by binding to lipid membranes (52–54). In AD patients, levels of soluble intracellular and membrane-associated Aβ in the temporal neocortex seem more closely related to AD symptoms than other measured Aβ species (55). Once again, our results are in line with the recent hypothesis that memory deficits correlate more strongly with cortical levels of soluble Aβ species than with insoluble Aβ plaque burden.

The potential mechanisms mediating the clearance of soluble Aβ by competent myeloid cells are numerous and might involve Aβ turnover, since CCR2 deficiency decreased the expression of neprilysin (Mme, a major Aβ-degrading enzyme) in the brain of AD mice (36). Bone marrow–derived microglial cells have the ability to phagocytize Aβ, and oligomeric, protofibrillar and fibrillar amyloid can be removed by microglia depending on the context (45,56–59). Although HSC-derived monocytic cells share common characteristics with microglia and peripheral monocytes, they reduce Aβ faster than microglia (60). These bone marrow–derived cells infiltrate into nonirradiated brain (61) and are genetically modified without compromising their function (60). Despite similar recruitment of microglia around Aβ plaques, APP$_{Swe}$/PS1 mice harboring CCR2$^{-/-}$ BMCs exhibited higher levels of soluble Aβ but similar Aβ deposition,

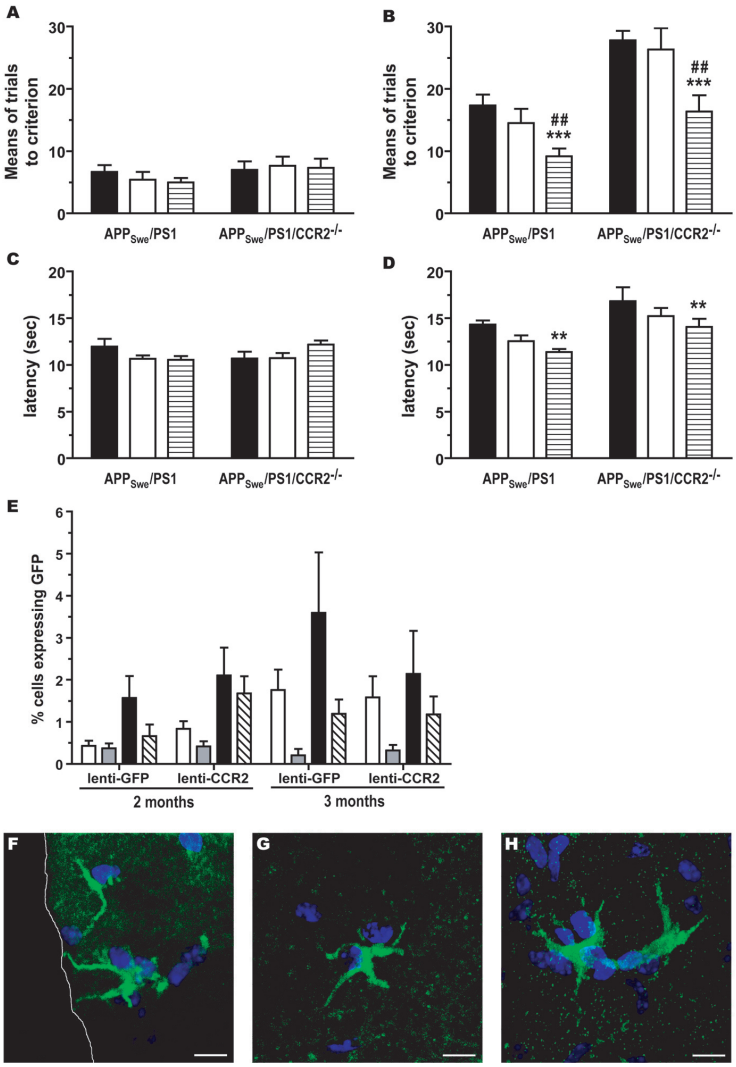

Figure 9. Treatment with lentivirus expressing the *CCR2* gene in the bone marrow rescues spatial memory in 6-month-old APP_{Swe}/PS1 and APP_{Swe}/PS1/$CCR2^{-/-}$ mice. Three-month-old APP_{Swe}/PS1 and APP_{Swe}/PS1/$CCR2^{-/-}$ mice received intrafemoral injections of a lentiviral construction containing GFP or GFP with a CCR2 transgene. At 6 months of age, mice were submitted to the water T-maze task. The number of trials to reach the criterion (A, B) and the time to arrive at the platform (C, D) were determined during the acquisition (A, C) and the reversal learning phases (B, D). Lenti-GFP-CCR2 treatment significantly decreased the number of trials and the time necessary to learn the platform position in APP_{Swe}/PS1/$CCR2^{-/-}$ mice, as well as in APP_{Swe}/PS1 mice. Interestingly, lenti-GFP-CCR2–treated mice had performances similar to WT mice. Results are expressed as the mean ± SEM; n = 6–13; $^{**}P < 0.01$ and $^{***}P < 0.001$ versus no treatment; $^{\#\#}P < 0.01$ versus lenti-GFP. Two-way ANOVA was performed and revealed no interaction between the various genotypes and treatments. Bonferroni or Tamhane tests were used for *post hoc* comparisons. Blood cells were analyzed by FACS, and GFP expression was detected in leukocytes 2 and 3 months after lenti-GFP or lenti-GFP-CCR2 intrafemoral injection (E). Among the various leukocyte populations, GFP protein was preferentially expressed in monocytes. Results are expressed as the mean ± SEM; n = 4–6. BMCs transduced with lenti-CCR2 infiltrated the brain parenchyma of nonirradiated APP_{Swe}/PS1/$CCR2^{-/-}$ mice, as depicted by confocal photomicrographs of the cerebral cortex (F, G) and hippocampus (H). Scale bar 10 μm. A–D: ■, No treatment; □, lenti-GFP; ▤, lenti-GFP-CCR2; E: □, total cells; ▩, lymphocytes; ■, monocytes; ▨, granulocytes.

suggesting that CCR2-deficient microglia do not phagocytize and clear soluble Aβ. Actually, disruption of Aβ clearance by microglia is probably the most important mechanism accounting for the accumulation of Aβ in a context of CCR2 deficiency. CCR2 deficiency in APP_{Swe}/PS1 mice was associated with higher CX_3CR1 expression levels in plaque-associated microglia concomitantly with enhanced levels of soluble Aβ (37). This result could explain the inability of $CCR2^{-/-}$ bone marrow–derived microglia to clear Aβ, since CX_3CR1/CX_3CL1 signaling strongly inhibits microglia activation and their phagocytic capacities (57,58). These effects could be also mediated by TGF-β1, since APP_{Swe}/PS1 mice harboring $CCR2^{-/-}$ BMCs exhibited enhanced expression of TGF-β1 and TGF-β-R1 and -R2 transcript levels in plaque-associated microglia. A drastic decrease in TGF-β1 and its receptor levels was found in microglia surrounding Aβ plaques in APP_{Swe}/PS1 and APP_{Swe}/PS1/$CCR2^{-/-}$ mice transplanted with WT GFP cells.

Although the exact role played by TGF-β1 in the physiopathology of AD is still debated today, accumulating evidence confirms its contribution to the progression of disease. *In vitro*, TGF-β1 binds Aβ with high affinity and induces Aβ oligomerization (62), whereas in the brain, TGF-β1 reduced microglial activation (63). TGF-β1 overexpression accelerates and promotes amyloidogenesis in mouse models of AD (64–66), and interruption of TGF-β1 signaling in BM-derived microglia/macrophages mitigates cognitive impairment and attenuates amyloidosis in AD mice (67). Therefore, TGF-β1 could act directly on microglia to diminish their phagocytic properties, prevent Aβ clearance and then increase Aβ production and oligomerization, which would aggravate memory deficits and accelerate disease progression. Here, again, a detrimental role of the TGF-β system was supported in the cognitive impairment and Aβ accumulation features, since diminution of brain soluble Aβ levels and restoration of

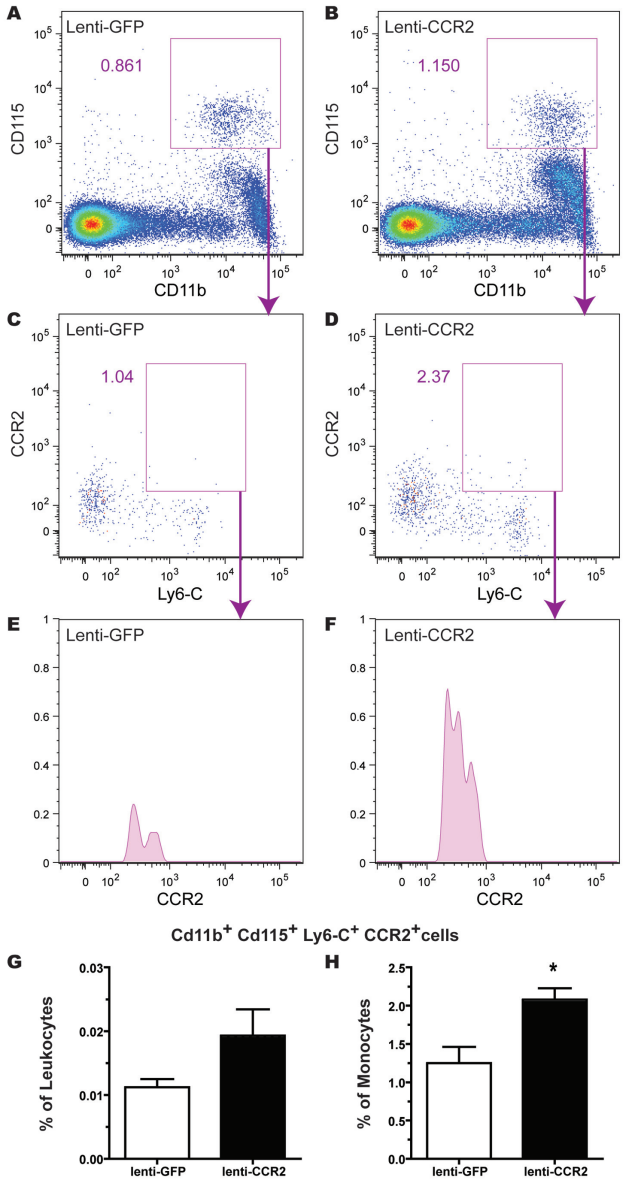

Figure 10. Treatment with lentivirus expressing the *CCR2* gene in the bone marrow induces CCR2 expression on the surface of Ly6-C$^+$ monocytes in CCR2$^{-/-}$ mice. Five-month-old CCR2$^{-/-}$ mice received intrafemoral injections of a lentiviral construction containing either GFP or GFP with a CCR2 transgene. Four weeks later, whole blood was stained with fluorescent antibody for CD11b, CD115, Ly6-C and CCR2 and analyzed by FACS. Monocytes were characterized by CD11b and CD115 expression in CCR2$^{-/-}$ mice injected with lenti-GFP (A) or lenti-GFP-CCR2 (B). In monocytes, Ly6-C and CCR2 expression was assessed in CCR2$^{-/-}$ mice injected with lenti-GFP (C) or lenti-GFP-CCR2 (D). Histograms (E, F) represent CCR2 signal in CD11b$^+$CD115$^+$Ly6-C$^+$CCR2$^+$ cells. Each graph shows a representative example of CCR2$^{-/-}$ mice injected with lenti-GFP (left column) or lenti-GFP-CCR2 (right column). Numbers near boxes indicate the percentage of CD11b$^+$ CD115$^+$ cells (A, B) or CD11b$^+$ CD115$^+$ Ly6-C$^+$ CCR2$^+$ cells (C, D) for this example. The percentage of CCR2$^+$ cells was determined in leukocytes (G) and monocytes (H). Interestingly, lenti-GFP-CCR2–treated mice exhibited CCR2 expression in leukocytes, which is significantly different in monocytes from control lenti-GFP–treated mice. Results are expressed as the mean ± SEM; n = 2–3; Student *t* test; *$P < 0.05$ versus lenti-GFP injected mice.

mnesic capacities were observed concomitantly with a reduction of TGF-β1 levels in APP mice transplanted with competent BMCs.

CCR2 is involved in CX$_3$CR1^{low}CCR2$^+$Gr1$^+$Ly6-C^{high} monocyte migration from bone marrow to bloodstream (20,21,49) and in the recruitment of monocytes, HSCs and hematopoietic progenitor cells into inflammatory tissues (19,22) as well as into brain (23–25). Surprisingly, microglia recruitment around Aβ plaque remained similar in APP$_{Swe}$/PS1 mice transplanted with WT or CCR2$^{-/-}$ BMCs. Despite the increase in MCP-1 expression in the brain of APP$_{Swe}$/PS1 mice transplanted with CCR2$^{-/-}$ BMCs, CCR2$^{-/-}$ cells cannot migrate in response to MCP-1 (36). Possible compensatory mechanisms may therefore take place in a context of CCR2 deficiency, and cell recruitment could imply other cytokines. It is important to note that bone marrow–derived microglia can originate from both CX$_3$CR1^{low}CCR2$^+$Gr1$^+$ and CX$_3$CR1^{high}CCR2$^-$Gr1$^-$ monocyte subsets, and we found that brain GFP cells exhibited variable CX$_3$CR1 expression levels, suggesting that both monocyte subsets have the ability to infiltrate the brain of AD mice. Lentivirus-containing CCR2 preferentially transduced cells of monocytic lineage, and these cells were later found in the brain of nonirradiated APP$_{Swe}$/PS1/CCR2$^{-/-}$ mice, allowing us to track CCR2$^+$ monocytes into the brain of AD mice without irradiation. Of great interest is the finding that the delivery of CCR2-expressing lentiviruses restored the monocyte populations and frequencies (for example, Gr1$^+$Ly6-C^{high} and Gr1$^-$Ly6-C^{low} subsets) in the blood, a procedure that was clearly beneficial in this mouse model of AD.

It was proposed that cerebral Aβ is cleared across the blood-brain barrier, based on the findings of active Aβ transport from the brain into the periphery via the low-density lipoprotein receptor (LRP-1) (68) and from the periphery into brain through the receptor for advanced glycation end products (69,70). The peripheral sink hypothesis proposes that a

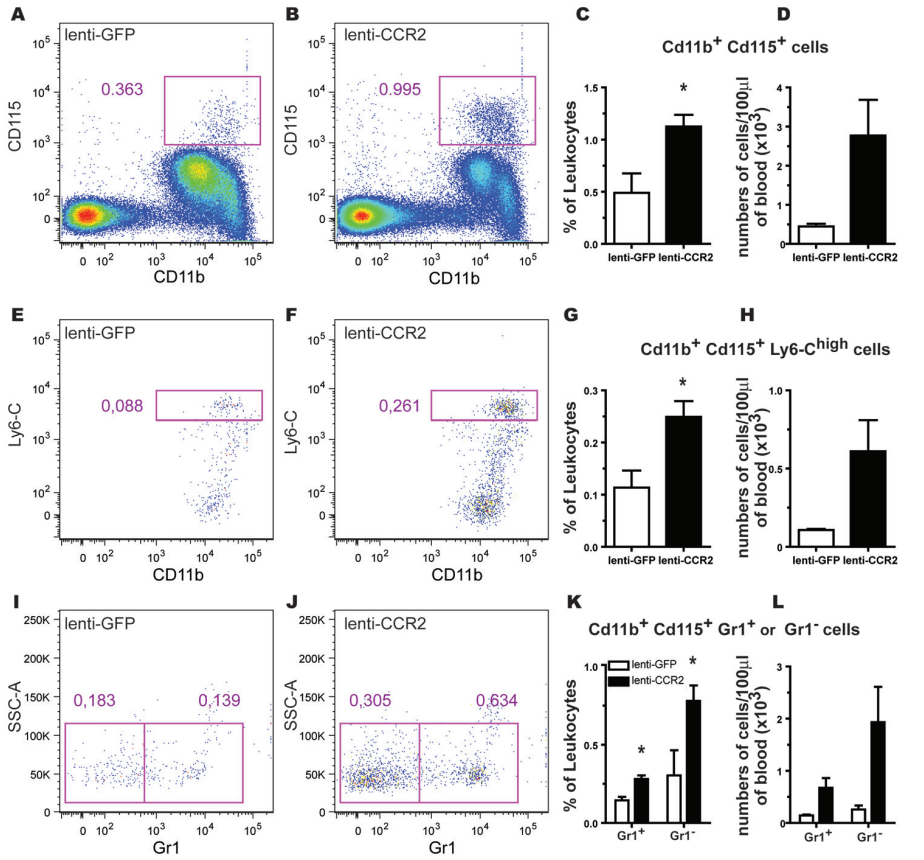

Figure 11. Treatment with lentivirus expressing a CCR2 transgene in the bone marrow increases the frequency of monocytes, especially in circulating Ly6-C$^+$, Gr1$^+$ and Gr1$^-$ subsets of CCR2$^{-/-}$ mice. Five-month-old CCR2$^{-/-}$ mice received intrafemoral injections of a lentiviral construction containing GFP or GFP with a CCR2 transgene. Three weeks later, CD11b, CD115, Ly6-C and Gr1 expression was analyzed by FACS in circulating leukocytes. Monocytes were characterized by CD11b and CD115 expression in CCR2$^{-/-}$ mice injected with lenti-GFP (A) or lenti-GFP-CCR2 (B). In monocytes, Ly6-C and CD11b expression was assessed in CCR2$^{-/-}$ mice injected with lenti-GFP (E) or lenti-GFP-CCR2 (F), as well as Gr1 expression (I and J, respectively). Intrafemoral injection of lenti-GFP-CCR2 increased the frequency of monocytes (CD11b$^+$ CD115$^+$ cells) (C, D), Ly6-C^{high} monocytes (G, H), as well as Gr1$^+$ and Gr1$^-$ monocytes (K, L). Each graph shows a representative example of CCR2$^{-/-}$ mice injected with lenti-GFP (left column) or lenti-GFP-CCR2 (middle column). Numbers near boxes indicate the percentage of CD11b$^+$ CD115$^+$ cells (A, B), CD11b$^+$ CD115$^+$ Ly6-C^{high} cells (E, F), as well as CD11b$^+$CD115$^+$ Gr1$^+$ or Gr1$^-$ cells (I, J) for this example. Results are expressed as the mean ± SEM; n = 2–3; Student *t* test; $^*P < 0.05$ versus lenti-GFP injected mice.

reduction of free Aβ levels in the blood enhances the transport of Aβ from the brain and then contributes to reduce the Aβ load in the brain (71–73). There is evidence for a dysfunctional brain-to-blood Aβ clearance in AD patients and in transgenic mouse models of the disease (70,71). CCR2-competent mononuclear cells could participate in the clearance of blood Aβ and then induce a dynamic export of soluble Aβ species out of the brain. Because CCR2 is required for monocytes to emigrate from the bone marrow (20–22,49), APP$_{Swe}$/PS1 mice transplanted with CCR2$^{-/-}$ BMCs presented a similar monocytopenia, as observed in CCR2$^{-/-}$ and APP$_{Swe}$/PS1/CCR2$^{-/-}$ mice. Both CX$_3$CR1^{low}CCR2$^+$Gr1$^+$ and CX$_3$CR1^{high}CCR2$^-$Gr1$^-$ subsets were decreased in the bloodstream, and the Gr1$^+$/Gr1$^-$ monocyte ratio was inversed comparatively to WT APP$_{Swe}$/PS1 mice and APP$_{Swe}$/PS1 mice harboring WT BMCs. In contrast, transplantation of WT BMCs and lenti-CCR2 treatment restored the population of monocytes in APP$_{Swe}$/PS1 and APP$_{Swe}$/PS1/CCR2$^{-/-}$ mice. These CCR2$^+$ monocytes might therefore clear Aβ from the circulation and the brain, thus explaining their important beneficial effects in limiting the progression of AD.

CONCLUSION

In conclusion, we have demonstrated that CCR2 deficiency specifically in HSCs of AP$_{PSw}$e/PS1 mice provokes a rapid cognitive decline that closely correlates with the accumulation of soluble Ab oligomers in the brain and with robust mRNA expression of TGF–b1 and its receptor TGF–b-R2 in C$_X$3CR1-positive microglia. Rescue of CCR2 expression in BMCs provides direct evidence that CCR2-competent bone marrow–derived microglia can restrict Ab toxicity and restore cognitive functions. The complementary approaches used in this study support a neuroprotective role for CCR2-competent monocytes in the physiopathology of AD. We propose that such innate immune mechanisms may be deficient or suboptimal in AD patients; therefore, gene therapy upregulating *CCR2* gene expression in HSCs is likely to provide a novel treatment with great potential in the near future. A similar approach using lentiviral-mediated gene therapy of HSCs was recently used with great success in two 7-year-old boys suffering from a rare and fatal demyelinating brain disease (74).

ACKNOWLEDGMENTS

The Canadian Institutes in Health Research and Neuroscience Canada (Brain Repair Program) supported this research. G Naert was supported by a postdoctoral fellowship from the Alzheimer Society of Canada. S Rivest is a Canadian Research Chair in Neuroimmunology. We

acknowledge the contribution of Mohammed Filali, Martine Lessard, Paul Préfontaine, Denis Soulet and Marie-Michèle Plante for technical help. We are grateful to Matthias Mack (Universitätsklinikum Regensburg Innere Medizin II/Nephrologie-Transplantation, Regensburg, Germany) for the gift of the anti-CCR2 antibody (Ab MC-21).

DISCLOSURE

The authors declare that they have no competing interests as defined by *Molecular Medicine*, or other interests that might be perceived to influence the results and discussion reported in this paper.

REFERENCES

1. Lesne S, *et al.* (2006) A specific amyloid-beta protein assembly in the brain impairs memory. *Nature.* 440:352–7.
2. Haass C, Selkoe DJ. (2007) Soluble protein oligomers in neurodegeneration: lessons from the Alzheimer's amyloid beta-peptide. *Nat. Rev. Mol. Cell. Biol.* 8:101–12.
3. Selkoe DJ. (2002) Alzheimer's disease is a synaptic failure. *Science.* 298:789–91.
4. Perry VH, Gordon S. (1988) Macrophages and microglia in the nervous system. *Trends Neurosci.* 11:273–7.
5. Dickson DW, *et al.* (1988) Alzheimer's disease: a double-labeling immunohistochemical study of senile plaques. *Am. J. Pathol.* 132:86–101.
6. Haga S, Akai K, Ishii T. (1989) Demonstration of microglial cells in and around senile (neuritic) plaques in the Alzheimer brain: an immunohistochemical study using a novel monoclonal antibody. *Acta. Neuropathol.* 77:569–75.
7. Simard AR, Soulet D, Gowing G, Julien JP, Rivest S. (2006) Bone marrow-derived microglia play a critical role in restricting senile plaque formation in Alzheimer's disease. *Neuron.* 49:489–502.
8. Stalder AK, *et al.* (2005) Invasion of hematopoietic cells into the brain of amyloid precursor protein transgenic mice. *J. Neurosci.* 25:11125–32.
9. Malm TM, *et al.* (2005) Bone-marrow-derived cells contribute to the recruitment of microglial cells in response to beta-amyloid deposition in APP/PS1 double transgenic Alzheimer mice. *Neurobiol. Dis.* 18:134–42.
10. Kaur C, Ling EA, Wong WC. (1987) Origin and fate of neural macrophages in a stab wound of the brain of the young rat. *J. Anat.* 154:215–27.
11. Ling EA. (1979) Transformation of monocytes into amoeboid microglia in the corpus callosum of postnatal rats, as shown by labelling monocytes by carbon particles. *J. Anat.* 128:847–58.
12. Soulet D, Rivest S. (2008) Bone-marrow-derived microglia: myth or reality? *Curr. Opin. Pharmacol.* 8:508–18.
13. Geissmann F, Jung S, Littman DR. (2003) Blood monocytes consist of two principal subsets with distinct migratory properties. *Immunity.* 19:71–82.
14. Auffray C, *et al.* (2009) CX3CR1+ CD115+ CD135+ common macrophage/DC precursors and the role of CX3CR1 in their response to inflammation. *J. Exp. Med.* 206:595–606.
15. Charo IF, Ransohoff RM. (2006) The many roles of chemokines and chemokine receptors in inflammation. *N. Engl. J. Med.* 354:610–21.
16. Luster AD. (1998) Chemokines: chemotactic cytokines that mediate inflammation. *N. Engl. J. Med.* 338:436–45.
17. Mack M, *et al.* (2001) Expression and characterization of the chemokine receptors CCR2 and CCR5 in mice. *J. Immunol.* 166:4697–704.
18. Saederup N, *et al.* Selective chemokine receptor usage by central nervous system myeloid cells in CCR2-red fluorescent protein knock-in mice. *PLoS One.* 5:e13693.
19. Si Y, Tsou CL, Croft K, Charo IF. (2010) CCR2 mediates hematopoietic stem and progenitor cell trafficking to sites of inflammation in mice. *J. Clin. Invest.* 120:1192–203.
20. Engel DR, *et al.* (2008) CCR2 mediates homeostatic and inflammatory release of Gr1(high) monocytes from the bone marrow, but is dispensable for bladder infiltration in bacterial urinary tract infection. *J. Immunol.* 181:5579–86.
21. Serbina NV, Pamer EG. (2006) Monocyte emigration from bone marrow during bacterial infection requires signals mediated by chemokine receptor CCR2. *Nat. Immunol.* 7:311–7.
22. Tsou CL, *et al.* (2007) Critical roles for CCR2 and MCP-3 in monocyte mobilization from bone marrow and recruitment to inflammatory sites. *J. Clin. Invest.* 117:902–9.
23. Izikson L, Klein RS, Charo IF, Weiner HL, Luster AD. (2000) Resistance to experimental autoimmune encephalomyelitis in mice lacking the CC chemokine receptor (CCR)2. *J. Exp. Med.* 192:1075–80.
24. Babcock AA, Kuziel WA, Rivest S, Owens T. (2003) Chemokine expression by glial cells directs leukocytes to sites of axonal injury in the CNS. *J. Neurosci.* 23:7922–30.
25. D'Mello C, Le T, Swain MG. (2009) Cerebral microglia recruit monocytes into the brain in response to tumor necrosis factoralpha signaling during peripheral organ inflammation. *J. Neurosci.* 29:2089–102.
26. D'Ambrosio D, Panina-Bordignon P, Sinigaglia F. (2003) Chemokine receptors in inflammation: an overview. *J. Immunol. Meth.* 273:3–13.
27. Rollins BJ, Yoshimura T, Leonard EJ, Pober JS. (1990) Cytokine-activated human endothelial cells synthesize and secrete a monocyte chemoattractant, MCP-1/JE. *Am. J. Pathol.* 136:1229–33.
28. Cushing SD, *et al.* (1990) Minimally modified low density lipoprotein induces monocyte chemotactic protein 1 in human endothelial cells and smooth muscle cells. *Proc. Natl. Acad. Sci. U. S. A.* 87:5134–8.
29. Smits HA, *et al.* (2002) Amyloid-beta-induced chemokine production in primary human macrophages and astrocytes. *J. Neuroimmunol.* 127:160–8.
30. Glabinski AR, *et al.* (1996) Chemokine monocyte chemoattractant protein-1 is expressed by astrocytes after mechanical injury to the brain. *J. Immunol.* 156:4363–8.
31. El Khoury JB, *et al.* (2003) CD36 mediates the innate host response to beta-amyloid. *J. Exp. Med.* 197:1657–66.
32. Meda L, *et al.* (1995) Activation of microglial cells by beta-amyloid protein and interferon-gamma. *Nature.* 374:647–50.
33. Deshmane SL, Kremlev S, Amini S, Sawaya BE. (2009) Monocyte chemoattractant protein-1 (MCP-1): an overview. *J. Interferon Cytokine Res.* 29:313–26.
34. Ishizuka K, *et al.* (1997) Identification of monocyte chemoattractant protein-1 in senile plaques and reactive microglia of Alzheimer's disease. *Psych. Clin. Neurosci.* 51:135–8.
35. Grammas P, Ovase R. (2001) Inflammatory factors are elevated in brain microvessels in Alzheimer's disease. *Neurobiol. Aging.* 22:837–42.
36. El Khoury J, *et al.* (2007) Ccr2 deficiency impairs microglial accumulation and accelerates progression of Alzheimer-like disease. *Nat. Med.* 13:432–8.
37. Naert G, Rivest S. (2011) The role of microglial cell subsets in Alzheimer's disease. *Curr. Alzheimer Res.* 8:151–5.
38. Simard AR, Rivest S. (2006) Neuroprotective properties of the innate immune system and bone marrow stem cells in Alzheimer's disease. *Mol. Psychiatry.* 11:327–35.
39. Richard KL, Filali M, Prefontaine P, Rivest S. (2008) Toll-like receptor 2 acts as a natural innate immune receptor to clear amyloid beta 1–42 and delay the cognitive decline in a mouse model of Alzheimer's disease. *J. Neurosci.* 28:5784–93.
40. Nadeau S, Rivest S. (2000) Role of microglial-derived tumor necrosis factor in mediating CD14 transcription and nuclear factor kappa B activity in the brain during endotoxemia. *J. Neurosci.* 20:3456–68.
41. Laflamme N, Lacroix S, Rivest S. (1999) An essential role of interleukin-1beta in mediating NF-kappaB activity and COX-2 transcription in cells of the blood-brain barrier in response to a systemic and localized inflammation but not during endotoxemia. *J. Neurosci.* 19:10923–30.
42. Laflamme N, Rivest S. (2001) Toll-like receptor 4: the missing link of the cerebral innate immune response triggered by circulating gram-negative bacterial cell wall components. *FASEB J.* 15:155–63.
43. Naert G, Laflamme N, Rivest S. (2009) Toll-like receptor 2-independent and MyD88-dependent gene expression in the mouse brain. *J. Innate. Immun.* 1:480–93.
44. Paxinos G, Franklin KBJ. (2001) The mouse brain in stereotaxic coordinates. 2nd ed. San Diego: Academic Press. [186 pp].
45. Boissonneault V, *et al.* (2009) Powerful beneficial effects of macrophage colony-stimulating factor

on beta-amyloid deposition and cognitive impairment in Alzheimer's disease. *Brain.* 132:1078–92.
46. Lue LF, *et al.* (1999) Soluble amyloid beta peptide concentration as a predictor of synaptic change in Alzheimer's disease. *Am. J. Pathol.* 155:853–62.
47. McLean CA, *et al.* (1999) Soluble pool of Abeta amyloid as a determinant of severity of neurodegeneration in Alzheimer's disease. *Ann. Neurol.* 46:860–6.
48. Cheng IH, *et al.* (2007) Accelerating amyloid-beta fibrillization reduces oligomer levels and functional deficits in Alzheimer disease mouse models. *J. Biol. Chem.* 282:23818–28.
49. Jia T, *et al.* (2008) Additive roles for MCP-1 and MCP-3 in CCR2-mediated recruitment of inflammatory monocytes during Listeria monocytogenes infection. *J. Immunol.* 180:6846–53.
50. Lesne S, Kotilinek L, Ashe KH. (2008) Plaque-bearing mice with reduced levels of oligomeric amyloid-beta assemblies have intact memory function. *Neuroscience.* 151:745–9.
51. Cleary JP, *et al.* (2005) Natural oligomers of the amyloid-beta protein specifically disrupt cognitive function. *Nat. Neurosci.* 8:79–84.
52. Klyubin I, *et al.* (2008) Amyloid beta protein dimer-containing human CSF disrupts synaptic plasticity: prevention by systemic passive immunization. *J. Neurosci.* 28:4231–7.
53. Hung LW, *et al.* (2008) Amyloid-beta peptide (Abeta) neurotoxicity is modulated by the rate of peptide aggregation: Abeta dimers and trimers correlate with neurotoxicity. *J. Neurosci.* 28:11950–8.
54. Shankar GM, *et al.* (2008) Amyloid-beta protein dimers isolated directly from Alzheimer's brains impair synaptic plasticity and memory. *Nat. Med.* 14:837–42.
55. Steinerman JR, *et al.* (2008) Distinct pools of beta-amyloid in Alzheimer disease-affected brain: a clinicopathologic study. *Arch. Neurol.* 65:906–12.
56. Bolmont T, *et al.* (2008) Dynamics of the microglial/amyloid interaction indicate a role in plaque maintenance. *J. Neurosci.* 28:4283–92.
57. Lee S, *et al.* (2010) CX3CR1 deficiency alters microglial activation and reduces beta-amyloid deposition in two Alzheimer's disease mouse models. *Am. J. Pathol.* 177:2549–62.
58. Liu Z, Condello C, Schain A, Harb R, Grutzendler J. (2010) CX3CR1 in microglia regulates brain amyloid deposition through selective protofibrillar amyloid-beta phagocytosis. *J. Neurosci.* 30:17091–101.
59. Mandrekar S, *et al.* (2009) Microglia mediate the clearance of soluble Abeta through fluid phase macropinocytosis. *J. Neurosci.* 29:4252–62.
60. Magga J, *et al.* (2011) Production of monocytic cells from bone marrow stem cells: therapeutic usage in Alzheimer's disease. *J. Cell. Mol. Med.* 2011, Jul 21 [Epub ahead of print].
61. Lebson L, *et al.* (2010) Trafficking CD11b-positive blood cells deliver therapeutic genes to the brain of amyloid-depositing transgenic mice. *J. Neurosci.* 30:9651–8.
62. Mousseau DD, *et al.* (2003) A direct interaction between transforming growth factor (TGF)-betas and amyloid-beta protein affects fibrillogenesis in a TGF-beta receptor-independent manner. *J. Biol. Chem.* 278:38715–22.
63. Brionne TC, Tesseur I, Masliah E, Wyss-Coray T. (2003) Loss of TGF-beta 1 leads to increased neuronal cell death and microgliosis in mouse brain. *Neuron.* 40:1133–45.
64. Wyss-Coray T, Lin C, Sanan DA, Mucke L, Masliah E. (2000) Chronic overproduction of transforming growth factor-beta1 by astrocytes promotes Alzheimer's disease-like microvascular degeneration in transgenic mice. *Am. J. Path.* 156:139–50.
65. Wyss-Coray T, *et al.* (2001) TGF-beta1 promotes microglial amyloid-beta clearance and reduces plaque burden in transgenic mice. *Nat. Med.* 7:612–8.
66. Wyss-Coray T, *et al.* (1997) Amyloidogenic role of cytokine TGF-beta1 in transgenic mice and in Alzheimer's disease. *Nature.* 389:603–6.
67. Town T, *et al.* (2008) Blocking TGF-beta-Smad2/3 innate immune signaling mitigates Alzheimer-like pathology. *Nat. Med.* 14:681–7.
68. Deane R, *et al.* (2004) LRP/amyloid beta-peptide interaction mediates differential brain efflux of Abeta isoforms. *Neuron.* 43:333–44.
69. Shibata M, *et al.* (2000) Clearance of Alzheimer's amyloid-ss(1–40) peptide from brain by LDL receptor-related protein-1 at the blood-brain barrier. *J. Clin. Invest.* 106:1489–99.
70. Deane R, *et al.* (2003) RAGE mediates amyloid-beta peptide transport across the blood-brain barrier and accumulation in brain. *Nat. Med.* 9:907–13.
71. DeMattos RB, *et al.* (2001) Peripheral anti-A beta antibody alters CNS and plasma A beta clearance and decreases brain A beta burden in a mouse model of Alzheimer's disease. *Proc. Natl. Acad. Sci. U. S. A.* 98:8850–5.
72. Lemere CA, *et al.* (2003) Evidence for peripheral clearance of cerebral Abeta protein following chronic, active Abeta immunization in PSAPP mice. *Neurobiol. Dis.* 14:10–8.
73. Holtzman DM, Bales KR, Paul SM, DeMattos RB. (2002) Abeta immunization and anti-Abeta antibodies: potential therapies for the prevention and treatment of Alzheimer's disease. *Adv. Drug Deliv. Rev.* 54:1603–13.
74. Cartier N, *et al.* (2009) Hematopoietic stem cell gene therapy with a lentiviral vector in X-linked adrenoleukodystrophy. *Science* 326:818–23.